NASA/CR—2014-218328

Synthesis, Processing, and Characterization of Inorganic-Organic Hybrid Cross-Linked Silica, Organic Polyimide, and Inorganic Aluminosilicate Aerogels

Baochau N. Nguyen, Haiquan N. Guo, and Linda S. McCorkle
Ohio Aerospace Institute, Brook Park, Ohio

July 2014

NASA STI Program . . . in Profile

Since its founding, NASA has been dedicated to the advancement of aeronautics and space science. The NASA Scientific and Technical Information (STI) program plays a key part in helping NASA maintain this important role.

The NASA STI Program operates under the auspices of the Agency Chief Information Officer. It collects, organizes, provides for archiving, and disseminates NASA's STI. The NASA STI program provides access to the NASA Aeronautics and Space Database and its public interface, the NASA Technical Reports Server, thus providing one of the largest collections of aeronautical and space science STI in the world. Results are published in both non-NASA channels and by NASA in the NASA STI Report Series, which includes the following report types:

- TECHNICAL PUBLICATION. Reports of completed research or a major significant phase of research that present the results of NASA programs and include extensive data or theoretical analysis. Includes compilations of significant scientific and technical data and information deemed to be of continuing reference value. NASA counterpart of peer-reviewed formal professional papers but has less stringent limitations on manuscript length and extent of graphic presentations.

- TECHNICAL MEMORANDUM. Scientific and technical findings that are preliminary or of specialized interest, e.g., quick release reports, working papers, and bibliographies that contain minimal annotation. Does not contain extensive analysis.

- CONTRACTOR REPORT. Scientific and technical findings by NASA-sponsored contractors and grantees.

- CONFERENCE PUBLICATION. Collected papers from scientific and technical conferences, symposia, seminars, or other meetings sponsored or cosponsored by NASA.

- SPECIAL PUBLICATION. Scientific, technical, or historical information from NASA programs, projects, and missions, often concerned with subjects having substantial public interest.

- TECHNICAL TRANSLATION. English-language translations of foreign scientific and technical material pertinent to NASA's mission.

Specialized services also include creating custom thesauri, building customized databases, organizing and publishing research results.

For more information about the NASA STI program, see the following:

- Access the NASA STI program home page at *http://www.sti.nasa.gov*

- E-mail your question to *help@sti.nasa.gov*

- Fax your question to the NASA STI Information Desk at 443–757–5803

- Phone the NASA STI Information Desk at 443–757–5802

- Write to:
  STI Information Desk
  NASA Center for AeroSpace Information
  7115 Standard Drive
  Hanover, MD 21076–1320

NASA/CR—2014-218328

Synthesis, Processing, and Characterization of Inorganic-Organic Hybrid Cross-Linked Silica, Organic Polyimide, and Inorganic Aluminosilicate Aerogels

Baochau N. Nguyen, Haiquan N. Guo, and Linda S. McCorkle
Ohio Aerospace Institute, Brook Park, Ohio

Prepared under Contract NNC07BA13B, Task order NNC07TA79T

National Aeronautics and
Space Administration

Glenn Research Center
Cleveland, Ohio 44135

July 2014

Acknowledgments

The researchers would like to acknowledge the following people who contributed their efforts and help in the completion and success of the projects: Dr. Mary Ann B. Meador and Dr. Fran Hurwitz (NASA Glenn) for their leads in the projects, Dr. Felix A. Miranda (NASA Glenn) for his lead in the Low Dielectric Aerogel and Patch Light Weight Antenna projects; Dr. Fred W. Vankuels (Vantage Partners) and Dr. Carl H. Mueller (Qinetiq North America) for their contribution and support in the Low Dielectric Aerogel and Patch Light Weight Antenna projects. Dan A. Scheiman (OAI) for performing all the Fourier Transform Infrared Spectroscopy (FTIR), Differential Scanning Calorimetry (DSC), Thermal Gravimetric Analysis (TGA), TGA-FTIR, Pycnometry, and Gel Permeation Chromatography (GPC). Dan Haas (NASA Glenn) for operating the supercritical fluid extraction, Dr. Bart Hamilton, Dr. Jiao Guo, and Saurabh Batra from Professor Mukerrem Cakmak's research group at the University of Akron for the use of the film casting machine and help with the production of polyimide aerogel films. Derek Quade (NASA Glenn), Dr. Bart Hamilton, and Dr. Jiao Guo (University of Akron) for performing the compression and tensile tests on aerogel films. Anna Palczer (deceased) for running the BET surface area of aerogels and her training of the BET instrument. All interns from the LERCIP, MUST, INSPIRE, and USRP programs for their help in the projects. They are Marissa E. Tousley, Jenna Proudfoot, Alexandra Medoro, Victoria Arendt, Marcus Rhohovie, Sara Ercegovic, Anna Sandberg, Guilherme (William) Sprowl, Sheeba Bali, and Brittany Wilkewitz.

Level of Review: This material has been technically reviewed by NASA technical management OR expert reviewer(s).

Available from

NASA Center for Aerospace Information
7115 Standard Drive
Hanover, MD 21076–1320

National Technical Information Service
5301 Shawnee Road
Alexandria, VA 22312

Available electronically at http://www.sti.nasa.gov

Synthesis, Processing, and Characterization of Inorganic-Organic Hybrid Cross-Linked Silica, Organic Polyimide, and Inorganic Aluminosilicate Aerogels

Baochau N. Nguyen, Haiquan N. Guo, and Linda S. McCorkle
Ohio Aerospace Institute
Brook Park, Ohio 44142

Abstract

As aerospace applications become ever more demanding, novel insulation materials with lower thermal conductivity, lighter weight and higher use temperature are required to fit the aerospace application needs. Having nanopores and high porosity, aerogels are superior thermal insulators, among other things. The use of silica aerogels in general is quite restricted due to their inherent fragility, hygroscopic nature, and poor mechanical properties, especially in extreme aerospace environments. Our research goal is to develop aerogels with better mechanical and environmental stability for a variety of aeronautic and space applications including space suit insulation for planetary surface missions, insulation for inflatable structures for habitats, inflatable aerodynamic decelerators for entry, descent and landing (EDL) operations, and cryotank insulation for advance space propulsion systems. Different type of aerogels including organic-inorganic polymer reinforced (hybrid) silica-based aerogels, polyimide aerogels and inorganic aluminosilicate aerogels have been developed and examined.

Nomenclature

APTES	3-aminopropyltriethoxysiliane
BAPP	2,2-bis-(4-[4-aminophenoxy]phenyl)propane
BAX	bisaniline-*p*-xylidene
BPDA	3,3',4,4'-biphenyl tetracarboxylic danhydride
BTDA	3,3',4,4'-benzophenone tetracarboxylic dianhydride
BTMSH	1,6-bis(trimethoxysilyl)hexane
BTMSPA	bis(trimethoxysilylpropyl)amine
BTSPD	bis[3-triethoxysilyl)propyl]disulfide
DMBZ	2,2'-dimethylbenzidine
DOE	design of experiments
EDL	entry, descent, and landing (EDL)
EVA	extravehicular activity
FMW	formulated molecular weights

8’ HTT	8’ high temperature tunnel
LHLMEL	Laser Hardened Materials Experimental Lab
MTMS	methyltrimethoxysilane
NH_4OH	ammonium hydroxide
NMP	N-methylpyrolidinone
NMR	nuclear magnetic resonance
OAPS	octa(aminophenyl)silsesquioxane
ODA	4,4’-oxydianiline
PI-PU	polyimide-polyurea
PDMS	poly(dimethylsiloxane)
PO	propylene oxide
PPDA	p-phenylene diamine
SEM	scanning electron miscroscope
TAB	1,3,5-triaminophenoxybenzene
Td	temperature of decomposition
TEOS	tetraethoxyorthosilicate
TEM	transmission electron microscope
TGA	thermogravimetric analysis
TIP	titanium isopropoxide
TMOS	tetramethoxyorthosilicate
TPS	thermal protection system
VTMS	vinyltrimethoxysilane

Table of Contents

1. Background

Silica aerogels are among materials with the lowest density and thermal conductivity. Having nanostructure with high mesoporosity and good transparency, silica aerogels are potential candidates for various thermal, optical, catalysts, chromatographic systems, and acoustic applications.[1] These materials are also attractive for space applications including the Stardust program, vehicles, space suits, and insulated boxes containing the batteries and electronics for Mars rovers.[2-6] However, the use of aerogels has been restricted due to their inherent fragility, hygroscopic nature, and poor mechanical properties. Hence, they have been limited to exotic applications such as collecting hypervelocity particles from the tail of a comet in the Stardust Mission, and as thermal insulation on the Mars Rover.

An aerogel is a gel whose solvent is replaced by air while maintaining the solid network structure. Generally, silica aerogels are prepared by a sol-gel process, in which their sol colloidal particles have diameters in the range of 1-1000 nm. The process can be done either by one-step or two-step method. The sols undergo gelation, forming sponge-like, three dimensional networks with solvent filling the pores. An aerogel is obtained when solvent in the pores is replaced by air with little change in the network structure or the volume of the gel body. This step is typically done by supercritical fluid extraction.

It has been demonstrated that a conformal coating of polymer over the skeletal nanostructure of the silica gel can be formed by reacting di-isocyanate with silanol groups on the surface.[7] This improves the strength by as much as two orders of magnitude while only doubling the density over those of native or non-reinforced aerogels. In addition, the mesoporosity of these polymer reinforced aerogels is maintained, which also retains their superior insulation properties, as well as others. Incorporating a functional group such as amine, vinyl or free-radical initiator into a silica-based aerogel improves the reactivity toward isocyanates, and also expands the types of organic monomers that can be used as reinforcement to include epoxides, cyanoacrylates, polyimides or styrene.[7-9]

Our extensive studies focused on improving the elastic properties of cross-linked silica-based aerogels. The approach is to reduce some of the -O-Si-O- bonds in the silica backbone with bulky groups or flexible organic linkages such as vinyltrimethoxysilane (VTMS), 1, 6-bis(trimethoxysilyl)hexane (BTMSH), and/or bis(trimethoxysilylpropyl)amine (BTMSPA), etc. Having flexible units in the underlying silica structure and in combination with different conformal polymer coatings, the resulting aerogel products exhibit, not only improved mechanical strength, but also improved elastic properties.

Yet another use for flexible durable aerogels could be as part of an inflatable decelerator used to slow spacecraft for planetary entry, descent and landing (*EDL*).[4] *EDL* systems were used to successfully land six robotic missions on Mars from 1976 to 2008. These past systems employed a hard aeroshell heat shield and parachutes of 12-16 m in diameter. Future robotic and manned missions are much heavier and will require more drag for landing. Hence, new designs with much larger diameters (30-60 m) will be required. Inflatable decelerators would stow in a small space and deploy into a large area lightweight heat shield to survive reentry. Minimizing weight and thickness of the system as well as providing suitable insulation are important considerations.[10] Much attention has been on the development of all organic polymer aerogel, and specifically on cross-linked polyimide aerogels.

While polymer reinforced silica-based aerogels show improvements in mechanical elastic properties, and cross-linked polyimide aerogels have improved flexibility and high temperature capability , these materials are not suitable for applications at temperature above 600^{o}C. In contrast, aluminosilicate aerogels have higher sinter temperature than silica aerogels, allowing the application temperature to be higher than 800^{o}C.[11-13] Aluminosilicate aerogel composites,

using ceramic paper, ceramic felts, or oxide foams as reinforcements, do not change microstructure even after heat treatment around 1100°C.

Over the past six years, our work has focused on synthesizing, developing, processing, and characterizing different types of aerogels as mentioned above. Productions have also been scaled up for testing in different space applications including insulation for cryotanks, patch antennas, EDL systems, and industrial applications such as pipe wrapping, packing, construction, and thermal insulation for daily life.

2. Synthesis, Characterization, and Processing of Low Density Polymer Cross-linked Silica Aerogels (Publications 1, 19, 24 and 26)

2.1. Clay Reinforced Polyimide/Silica Hybrid Aerogels (Publication 1)

One of the polymers of interest cross-link silica aerogel is polyimide. Polyimides are high performance polymers and widely used as matrix resins in fiber reinforced composites. Aromatic polyimides, in particular, are known to have exceptional thermal oxidative stability, excellent mechanical and electrical properties, good chemical resistance in most common solvents, and low dielectric constant. Fabrication of polyimides as conformal coatings over the native silica aerogels provides a better overall structural integrity. Shown in Scheme 1 is the chemical reaction of the polyimide. In this method, a polyimide was introduced to the silica network as a bridge between silica particles to improve the structural integrity. In addition, exfoliated clay was also incorporated to reinforce the aerogel matrix. Table 1 shows the physical properties of the final products at various amounts of clay.

The clay/hybrid system was prepared using one-step synthesis, where exfoliated clay was incorporated in the amic acid silica sol-gels before the imidization reaction took place. Layered silicate clays are an exceptionally stable oxide network with plate-like morphology, high surface area, and high in-plane strength, thus, well suited for polymer/silica hybrid composite systems.

The clay reinforced hybrid silica aerogels exhibited ranges of density, shrinkage, and porosity similar to the non-reinforced aerogel. However, their BET surface areas were lower probably due to larger pore diameter and wider pore size distribution. Compared to the non-reinforced aerogels, compression moduli of clay reinforced aerogels are higher, ranging from 8 – 21 MPa. Under transmission electron microscope (TEM) graphs, silica particles appeared to grow from the edges of the well dispersed clay pallets from which the OH functionalized groups from both the clay and silica aerogels formed covalent and hydrogen bonds with each other, substantially reinforcing the network structure.

Table 1. Physical properties of polyimide/silica hybrid aerogels reinforced with STN clay.

Clay %	Density g/cm3	Shrinkage %	Porosity %	BET surface area g/m2
0	0.28	30.7	82	504
1	0.22	35.3	85	446
2	0.27	29.2	87	376
3	0.22	23.8	88	378
4	0.27	28.4	84	501
5	0.26	24.1	87	428
6	0.30	26.8	84	406

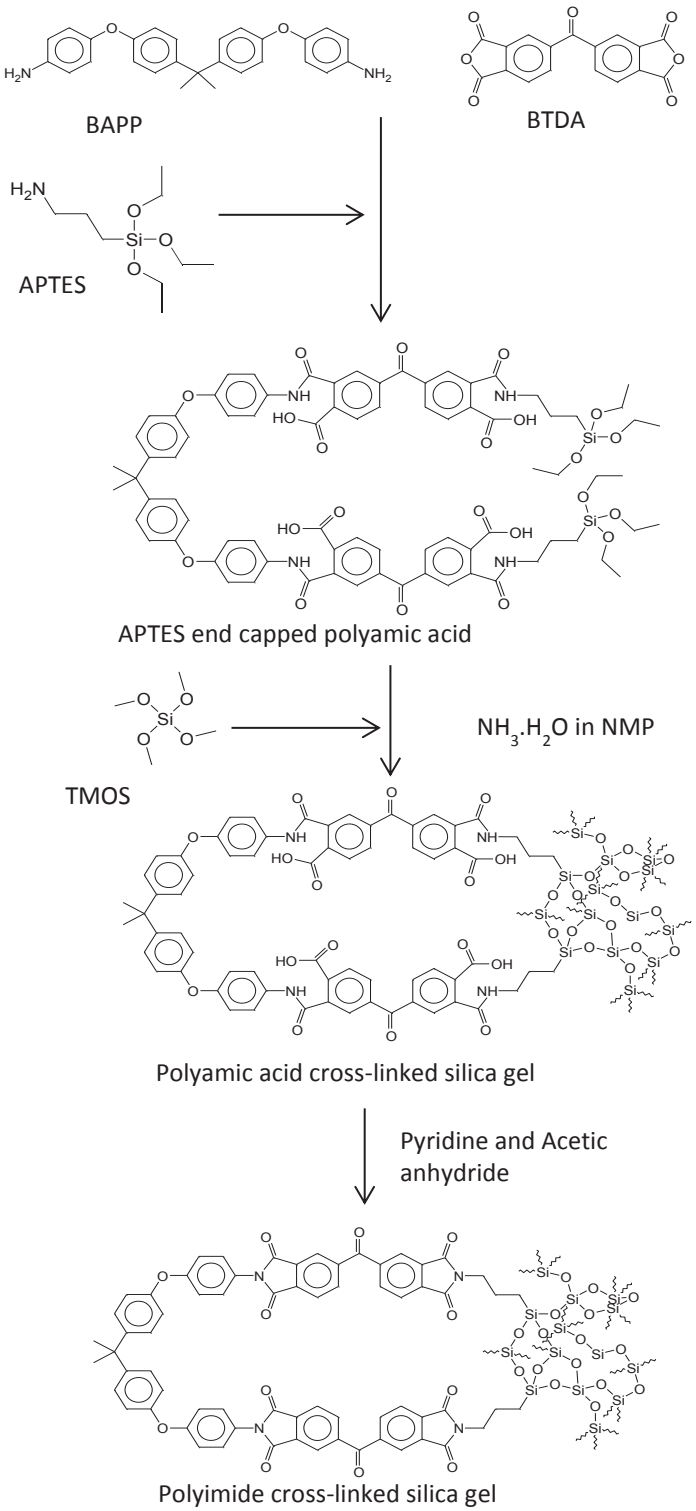

Scheme 1. Chemical reaction of polyimide/silica hybrid aerogel (Reproduced from Publication 1 with permission from The Royal Society of Chemistry).

2.2. Synthesis, Characterization, and Processing of Flexible Organic-Inorganic Hybrid Aerogels (Publications 19, 24, and 26)

Silica aerogels made with tetra-alkylorthosilicate precursors, such as tetramethoxyorthosilicate (TMOS) or tetraethoxyorthosilicate (TEOS), tend to form a stiff, brittle silica network. Though some measure of flexibility is obtained in the polymer reinforced aerogels through a decrease in density, it has been shown that more flexibility is obtained in unreinforced aerogels by altering the silica back-bone in some significant way. For example, Kramer et al demonstrated that including up to 20% (w/w) poly(dimethylsiloxane) (PDMS) in TEOS–based aerogels resulted in rubbery behavior with up to 30% recoverable compressive strain. More recently, Rao and Kanamori showed that aerogels synthesized using methyltrimethoxysilane (MTMS) by virtue of less Si–O–Si bonding can be flexible, and recover or spring back after compression. Another method of improving flexibility or elastic recovery in aerogels is to include organic linking groups in the underlying silica structure. Shea and Loy have fabricated hybrid organic-inorganic aerogels from bridged polysilsesquioxanes, using building blocks comprised of organic bridges attached to two or more trialkoxysilyl groups via non-hydrolyzable carbon-silicon bonds. The properties of the silsesquioxane derived aerogels, including mechanical properties and pore structure, depend in large part on the size and stiffness of the organic bridges.

2.2.1. Silica-based Aerogels Cross-linked with Polystyrene (Publication 26)

While aromatic containing bridges, such as aromatic polyimides, are stiffer and provide excellent control over pore size and distribution of pores, alkylene-bridged polysilsesquioxane aerogels, in contrast, tend to be more flexible, more compliant aerogels but tend to shrink more, reducing porosity.

To counteract this, the effect of incorporating an organic linking group such as 1,6-bis(trimethoxysilyl)hexane (BTMSH), into the underlying silica structure was examined. Vinyltrimethoxysilane (VTMS) is also incorporated as a site for styrene cross-linking in these gels. Schemes 2 and 3 are proposed molecular structures of the unreinforced silica-based aerogels and a proposed cross-linking of styrene with VTMS, respectively. A design of experiment (DOE) (Table 2) was employed. The effect of four variables used in the preparation of the aerogels, including the total concentration of silicon (derived from TMOS, VTMS, and BTMSH combined), mol % of VTMS, mol % of BTMSH, and polystyrene formulated molecular weights (FMW) on mechanical and other properties of the aerogels was evaluated.

As one may expect, increasing total Si results in higher density due to a denser backbone. A similar effect is also observed with increasing amount of VTMS, which provides more vinyl sites for cross-linking with styrene. However, incorporation of BTMSH causes a decrease in density. This is probably due to the vinyl groups being sterically hindered by BTMSH, thus decreasing the amount of styrene to react.

The density is also influenced by dimensional shrinkage over the course of processing the aerogels. Overall, VTMS fraction and polystyrene FMW have the greatest effect on shrinkage. High VTMS fraction and high polystyrene FMW reduce shrinkage by reinforcing the silica backbone through increasing the amount of polymer crosslinking. On the other hand, low shrinkage is also observed when the total Si and the fraction of BTMSH derived Si are high. This is most likely due to the effect of the phase separation occurring in these formulations, making the silica backbone and the pore sizes larger and thus, less prone to collapse.

From the study, it was found that modulus increases with increasing total silicon concentration as this leads to higher densities. Surprisingly, modulus decreases with increasing fraction of VTMS even though this increases the number of sites available for cross-linking.

However, increasing VTMS also tends to make the silica backbone less stiff due to less siloxyl bonding (Figure 1). As expected, increasing amount of BTMSH also leads to a decreas in modulus, likely due to the effect of introducing more flexible links into the silica backbone, but also due to the fact that at very high loadings, the hexyl groups inhibit cross-linking. Such evidence of unreacted vinyl groups from VTMS has been verified using ^{13}C nuclear magnetic resonance (^{13}C NMR).

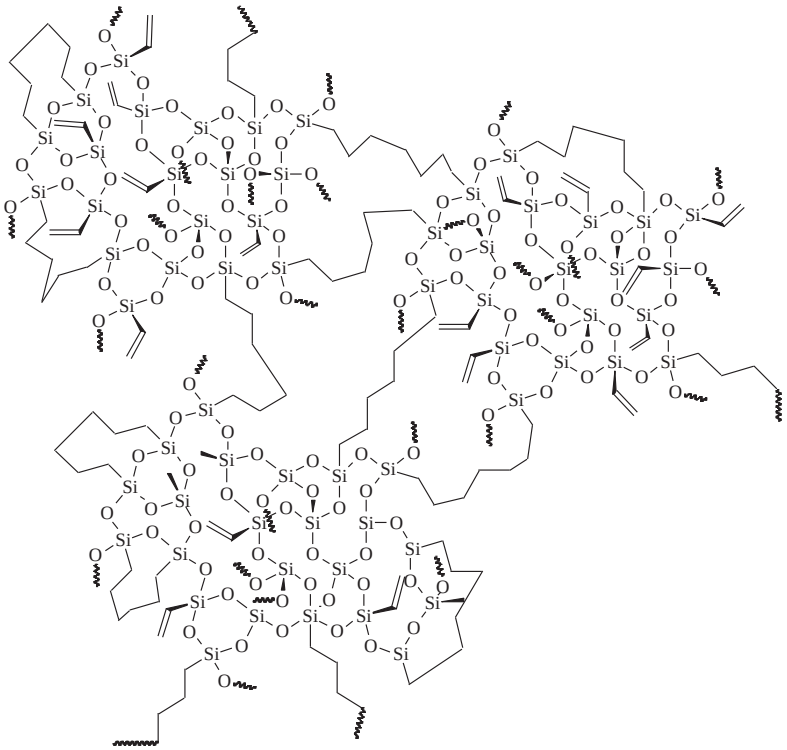

Scheme 2. Proposed molecular structure of silica gel made from approximately 28% VTMS and 40% BTMSH (Reprinted with permission from Publication 26. Copyright 2009 American Chemical Society).

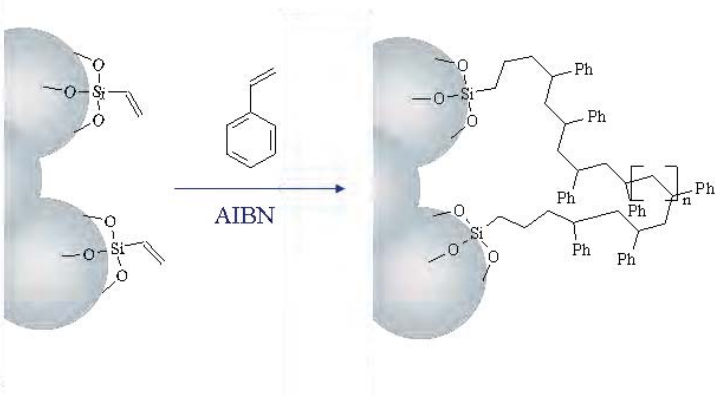

Scheme 3. Proposed cross-linking of VTMS and styrene (Reprinted with permission from Publication 26. Copyright 2009 American Chemical Society).

Table 2. Preparation conditions and properties of polystyrene cross-linked silica-based aerogels (Reprinted with permission from Publication 26. Copyright 2009 American Chemical Society).

Formulation	Total Si, M	Water:Silane	VTMS, mol%	BTMSH, mol%	Polystyrene, MW	Gelation Solvent	Bulk Density, g/cm^3	Porosity, %	Shrinkage,%	Modulus, MPA	Unrecovered strain, %	Contact Angle, °	BET Surface Area, m^2/g	T_d, °C in N_2
1	1.49	8.5	20	30	1500	MeOH	0.327	76.8	25.0	17.54	9.50	133.4	576	278.4
2	1.25	7.7	40	48	2500	MeOH	0.175	85.9	10.0	0.47	1.55	125.1	8	266.5
3	1.68	8.7	42	0	500	MeOH	0.330	76.6	20.0	20.35	10.00	114.6	667	294.9
4	1.61	9.1	25	0	2500	MeOH	0.327	77.3	22.0	20.00	9.50	112.2	640	322.2
5	1.82	7.8	29	49	2500	MeOH	0.232	82.3	8.5	3.29	0.45	137.4	158	263.2
6	1.82	5.2	29	49	2500	MeOH	0.241	81.7	9.0	1.07	1.95	137.0	95	270.0
7	2.05	8.1	34	29	1500	MeOH	0.284	78.6	10.5	10.68	8.15	138.3	550	283.1
8	1.25	7.7	40	48	1500	MeOH	0.172	86.2	10.0	0.23	2.65	131.9	8	271.5
9	1.98	8.4	20	30	500	MeOH	0.370	70.6	20.0	32.43	11.10	127.0	751	279.9
10	1.06	8.1	47	28	500	MeOH	0.122	90.3	5.5	0.17	9.90	125.3	366	287.3
11	0.99	8.7	20	30	2500	MeOH	0.309	77.9	33.5	18.04	6.70	133.7	601	278.7
12	1.82	7.8	29	49	500	MeOH	0.243	81.2	8.5	2.42	1.00	127.4	6	274.3
13	1.82	5.2	29	49	500	MeOH	0.250	80.9	9.0	0.87	1.30	135.2	70	263.3
14	1.06	8.1	47	28	500	MeOH	0.125	90.3	6.5	0.20	8.40	132.2	372	279.5
15	1.25	7.7	40	48	2500	EtOH	0.197	84.7	13.0	1.45	8.30	130.9	311	305.7
16	1.25	7.7	40	48	1500	EtOH	0.210	83.7	15.5	1.44	9.75	134.0	277	305.5
17	1.82	7.8	29	49	500	EtOH	0.244	81.7	8.0	1.8	1.35	137.8	221	312.0

As a way of measuring elastic properties, aerogel monoliths were taken through two successive compression cycles to 25% strain. Two sample stress-strain curves from these tests are shown in Figure 2a (formulation 5) for a monolith with a high degree of recovery after compression (low unrecovered strain) and in Figure 2b (formulation 10) for a monolith with a lower degree of recovery. Note how the first and second compression curves nearly retrace each other in Figure 2a while in Figure 2b, the second curve does not start to rise until about 10% strain. This amount represents the loss of sample length after the first compression. Figure 3 shows a picture of the aerogel monolith made from formulation 5 before the test and after two compression cycles, showing that the sample length has changed very little through the course of the test.

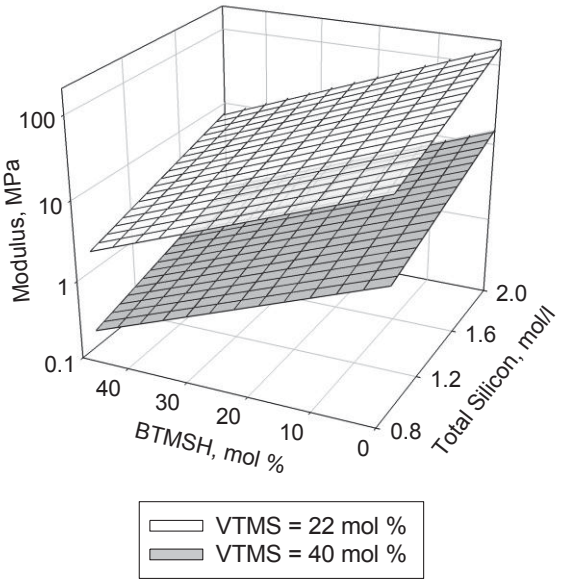

Figure 1. Response surface model for modulus plotted vs. total silicon concentration and BTMSH-derived Si mol % (Reprinted with permission from Publication 26. Copyright 2009 American Chemical Society).

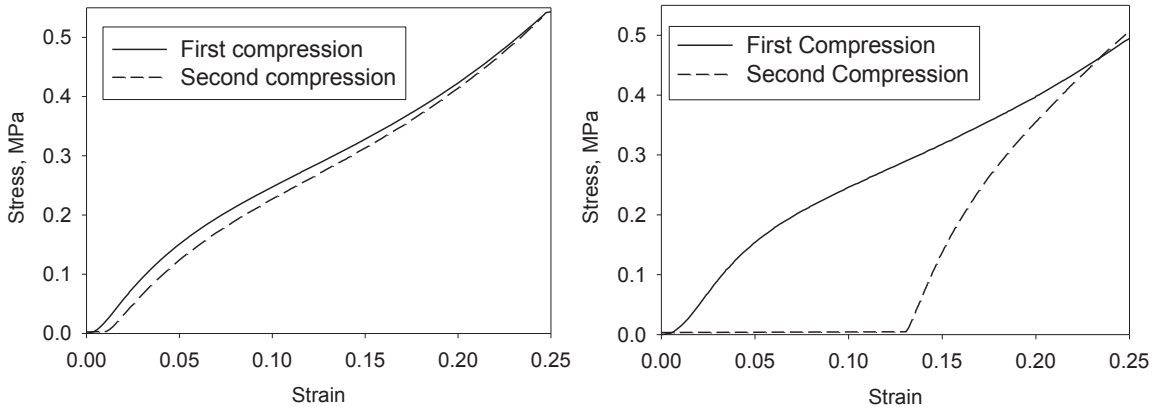

Figure 2. Typical stress-strain curves for a repeat compression tests on a) formulation 5 with 49 mol% BTMSH and b) formulation 10 with 28 mol% BTMSH (Reprinted with permission from Publication 26. Copyright 2009 American Chemical Society).

Contact angles measured in this study ranged from 112-114 ° for samples containing no BTMSH to 127-138 ° for samples with at least 29 mol % BTMSH Si as listed in Table 2. This indicates that the hexyl group from BTMSH is present on the silica surface, and has a significant effect on the hydrophobic nature of the aerogels above and beyond the styrene cross-linking.

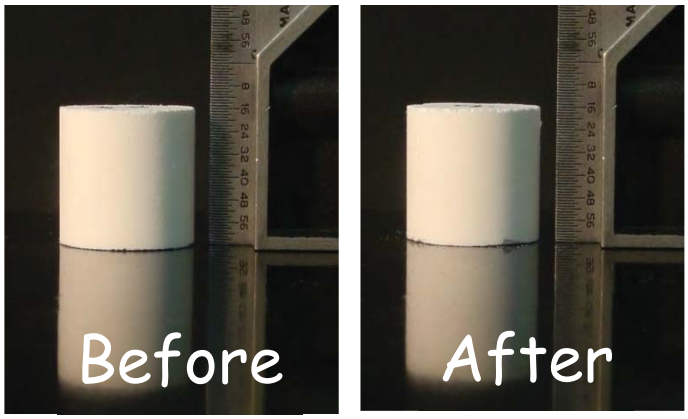

Figure 3. Monolith from formulation 5 shown before and after two compression cycles (Reprinted with permission from Publication 26. Copyright 2009 American Chemical Society).

A study of the solubility and homogeneity between solvent and the precursors was conducted with methanol and ethanol. High BTMSH containing aerogels prepared from methanol exhibit phase separation which lead to the loss of mesoporosity and hence, low surface areas as a consequence. Ethanol, being a less polar solvent than methanol and having a higher alkyl chain, better solvates the vinyl and hexyl group on the surface of the developing silica particles, and helps keep a more homogeneous or continuous phase. Illustrated in Figure 4 are micrographs of pairs of samples prepared in methanol and ethanol. Dramatic changes in microstructures could be seen, and formulations prepared in ethanol produce a more uniform, finer particle structure than those from methanol, resulting in higher surface areas, from 6 - 8 m^2/g to 220 - 311 m^2/g.

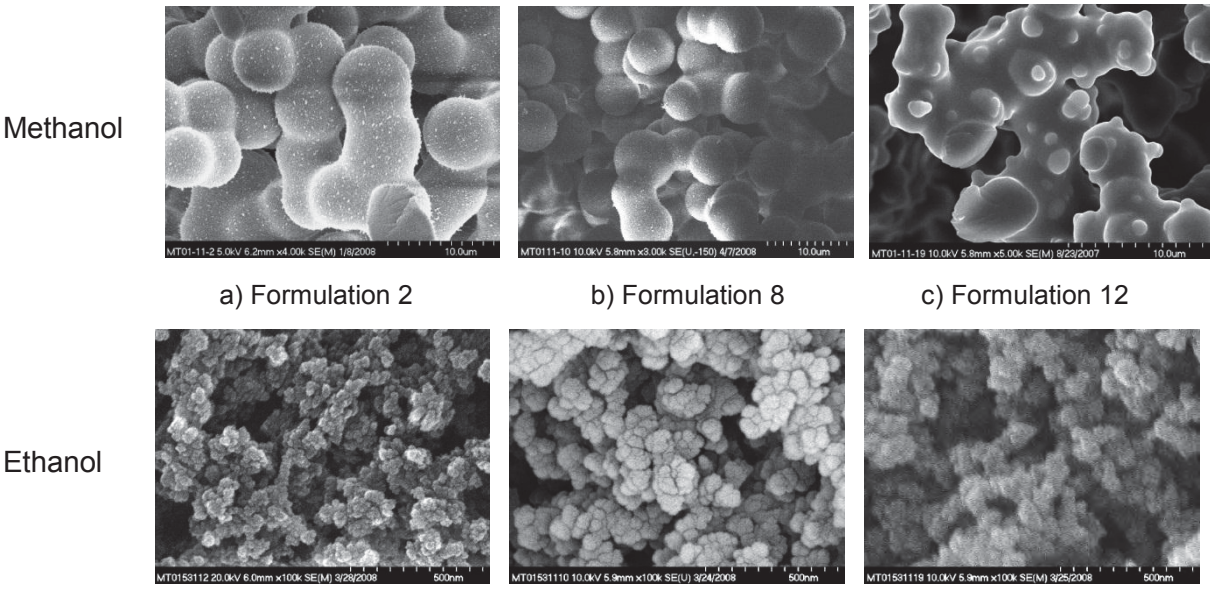

Figure 4. Scanning electron microscope (SEM) images of aerogel monoliths prepared from (upper) methanol solution (a – c) and (lower) ethanol solution (d – f) (Reprinted with permission from Publication 26. Copyright 2009 American Chemical Society).

2.2.2. Elastic behavior of Methyltrimethoxysilane Based-Aerogels Reinforced with Tri-isocyanate (Publication 19)

Though MTMS derived aerogels are very flexible and elastic, it does not take much force to compress them. Similar to the above approach where VTMS and BTMSH with flexible linkages, were incorporated into the underlying silica structure and co-reacted with TMOS, the aerogels in this study were prepared using MTMS and bis(trimethoxysilylpropyl)amine (BTMSPA) precursors in a one–step synthesis. The secondary amine from the BTMSPA is used as base to catalyze condensation of the silanes, as well as a cross-linking site for reaction to form a polyurea conformal coating on the silica structure. A statistical experimental design is employed to examine the effect of four variables used in the preparation of the aerogels, including the total concentration of silicon (derived from MTMS and BTMSPA combined), mol % BTMSPA, water/silicon mol ratio, *r*, and the number of washes (removal of excess water in the hydro gels) before the cross–linking with a tri-isocyanate, Desmodur N3300A, on mechanical and other properties of the aerogels. Properties of these polymer reinforced aerogels are also compared to their non–cross–linked counterparts. The effect of solvents including acetonitrile and acetone on the properties was also investigated (Tables 3 and 4). Shown in Schemes 4 and 5 are the proposed molecular structure of the polymer reinforced aerogels and the reaction of water with isocyanate.

As one may expect, densities of both non-reinforced and polymer reinforced samples increase with increasing total silicon concentration as well as increasing mol fraction of BTMSPA. This is due to the addition of more silica to the structure and more organic linking groups to the backbone. For the cross-linked aerogels, a higher fraction of BTMSPA introduces more amine sites available for tri-isocyanate reaction. However, as found in this study, very little polymer is incorporated in formulations with the lowest total silicon and BTMSPA fraction, yielding insignificant increase in density compared to their non-cross-linked counterparts. Again, the density and porosity are also influence by the dimensional change or shrinkage (%) of the monolith. In general, higher shrinkage results in higher density and low porosity (%). Overall, as reported in Table 3, the polymer cross-linked network appears to retain the pore structure, or BET surface areas, better than the non-cross-linked system (Table 4). The polymer reinforced aerogels tends to shrink 2 - 3 % less than their non-reinforced counterparts, and those prepared in acetonitrile shrink 1 – 2 % less than those made in acetone.

SEM images of select samples from the study are shown in Figure 5 to illustrate the differing morphologies arising from different processing conditions. Non-reinforced aerogels shown in Figure 5 a-c illustrate the increase in particle size and decrease in surface area as total Si and BTMSPA fraction is reduced. A similar trend is observed in the polymer cross-linked aerogels (Figure 5 d-i). At high Si concentration, denser structures, higher densities, and lower BET surface areas in the reinforced specimens prove the presence of tri-isocyanate in the system, especially when prepared using acetone as solvent, indicating the more available amine sites for the cross-linking reaction. At the lowest Si concentration in this study, much larger particle sizes formed, which are smoother in appearance, indicating the loss of the fine pore structure, as well as almost no tri-isocyanate incorporated, evidenced by ^{13}C NMR (Figure 6). Note that the scale for those at low concentration (Figure 6 c, f, and i) is at a much lower magnification.

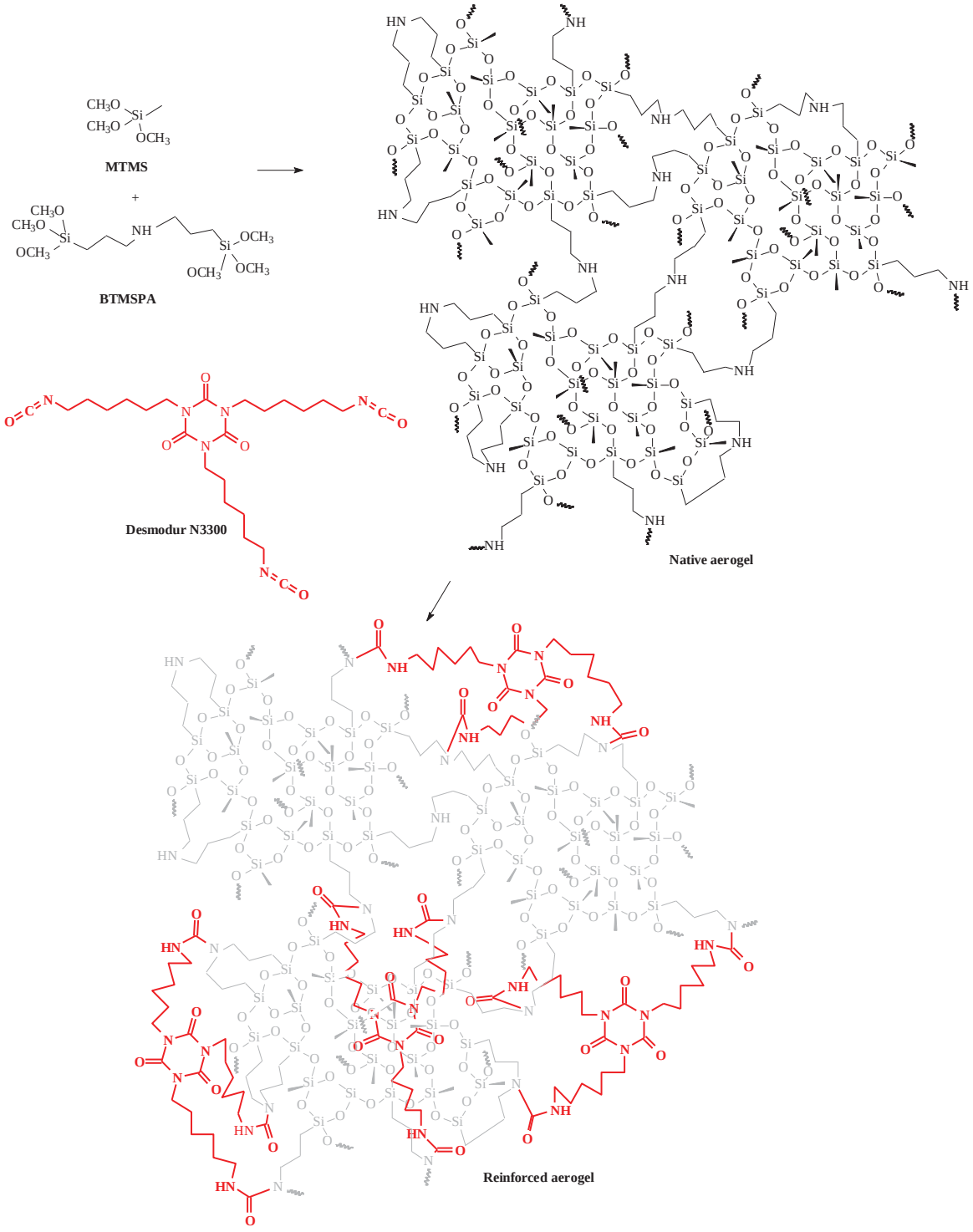

Scheme 4. Proposed molecular structure of aerogels from MTMS and BTMSPA reinforced with tri-isocyanate Desmodur N3300 (Reprinted with permission from Publication 19. Copyright 2010 American Chemical Society).

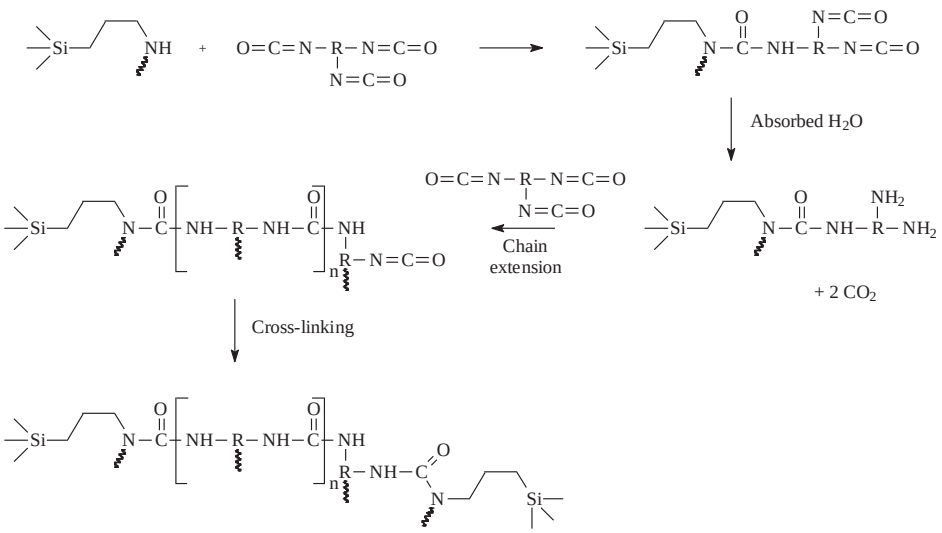

Scheme 5. Mechanism for cross-linking reaction of amine with tri-isocyanate, including chain extension reaction due to excess water (Reprinted with permission from Publication 19. Copyright 2010 American Chemical Society).

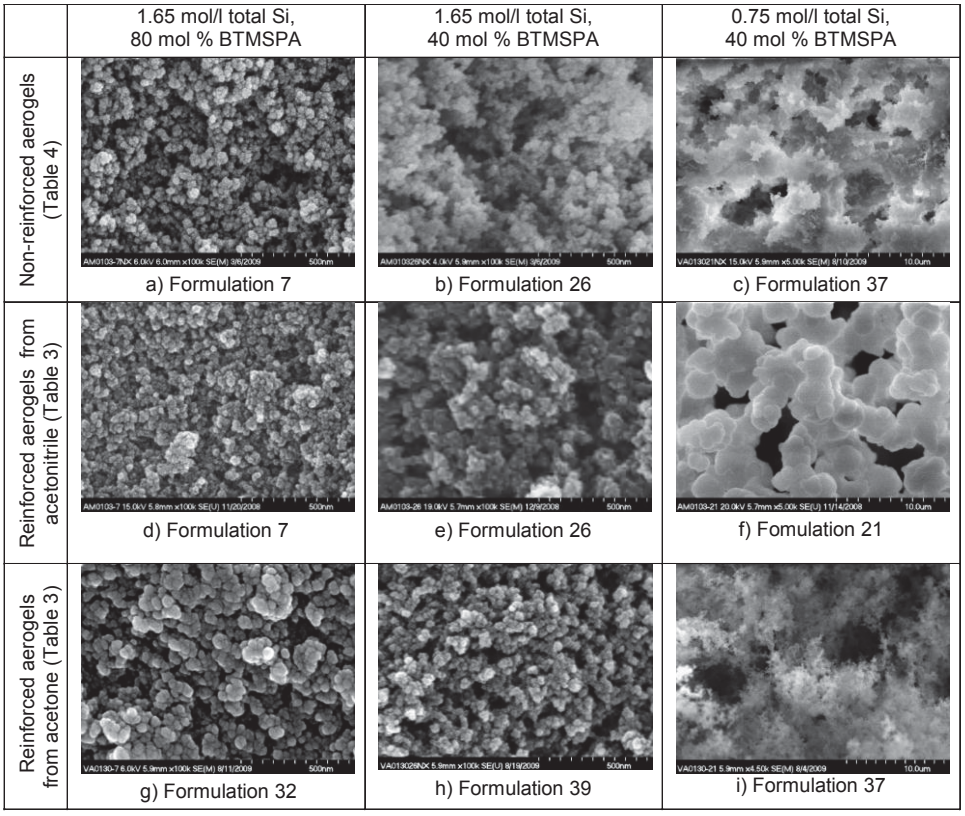

Figure 5. SEM images of select non-reinforced samples (a, b, and c) from Table 4, compared to corresponding reinforced aerogels from Table 3 prepared using acetonitrile as solvent (d, e, and f), and using acetone as solvent (g, h, and i) (Reprinted with permission from Publication 19. Copyright 2010 American Chemical Society).

Table 3. Preparation conditions and measured properties for polymer reinforced aerogels (Reprinted with permission from Publication 19. Copyright 2010 American Chemical Society).

Formulation #	Total Si, M	MTMS, mol%	BTMSPA, mol%	Water: Silane	# of Washes	Solvent	NCO:NH ratio	Bulk Density, g/cm^3	Porosity, %	Shrinkage,%	BET Surface Area m^2/g	Modulus, MPa	Max. Stress at Break, MPa	Toughness, kJ/m^3	Unrecovered strain, %
1	0.75	60	40	2.0	1	acetonitrile	0.03	0.058	95.9	4.0	a	0.00	2.76E-3	0.4	1.6
2	1.20	40	60	3.5	2	acetonitrile	0.71	0.163	87.9	2.0	230.5	2.60	3.8	582	1.0
3	1.20	40	60	3.5	3	acetonitrile	0.71	0.160	88.5	2.0	237.6	2.69	4.1	631	1.1
4	1.65	20	80	5.0	3	acetonitrile	1.02	0.369	72.1	10.2	260.0	72.36	36.7	6488	2.1
5	0.75	20	80	5.0	3	acetonitrile	0.58	0.101	92.6	3.1	139.1	0.60	0.3	47	0.7
6	1.65	60	40	2.0	1	acetonitrile	0.72	0.187	85.8	1.2	292.3	2.94	4.3	662	3.2
7	1.65	20	80	5.0	1	acetonitrile	1.22	0.385	70.6	9.6	233.5	84.25	39.7	6944	3.0
8	1.20	40	60	5.0	2	acetonitrile	0.82	0.167	87.8	2.1	204.9	3.51	3.4	524	1.1
9	1.20	40	60	3.5	1	acetonitrile	0.94	0.163	90.2	2.1	203.9	3.12	2.6	437	0.7
10	1.20	40	60	2.0	2	acetonitrile	0.95	0.157	89.6	1.7	234.1	2.26	3.7	556	0.5
11	0.75	40	60	3.5	2	acetonitrile	0.05	0.072	95.4	2.0	18.1	0.02	0.0	5.1	1.1
12	1.20	40	60	3.5	2	acetonitrile	0.94	0.164	87.8	1.6	233.6	2.48	3.1	477	1.8
13	1.20	20	80	3.5	2	acetonitrile	1.01	0.216	84.2	4.9	248.1	10.55	12.3	1893	1.1
14	1.20	40	60	3.5	2	acetonitrile	0.77	0.157	88.5	1.8	231.6	2.74	2.9	448	1.3
15	1.20	40	60	3.5	2	acetonitrile	0.88	0.159	88.1	1.5	224.6	2.68	3.4	2085	0.7
16	0.75	20	80	2.0	1	acetonitrile	0.39	0.102	92.7	2.4	93.2	0.32	0.9	115	0.7
17	1.20	40	60	3.5	2	acetonitrile	0.69	0.160	88.5	2.2	229.1	2.38	2.8	383	0.7
18	1.20	40	60	3.5	2	acetonitrile	0.89	0.219	83.6	1.6	217.9	2.77	4.6	687	1.3
19	0.75	60	40	5.0	3	acetonitrile	0.01	0.053	96.9	2.8	a	0.01	9.7E-3	2.2	0.0
20	1.65	20	80	2.0	1	acetonitrile	1.03	0.356	72.9	8.9	266.1	49.98	41.9	6988	2.2
21	0.75	60	40	5.0	1	acetonitrile	0.01	0.049	97.0	1.9	7.4	0.01	1.0E-3	1.9	0.0
22	0.75	20	80	5.0	1	acetonitrile	0.50	0.105	92.6	2.3	126.2	0.50	0.4	71	0.6
23	1.65	60	40	5.0	3	acetonitrile	0.74	0.185	86.3	1.3	275.6	2.65	2.8	426	2.6
24	0.75	20	80	2.0	3	acetonitrile	0.46	0.100	92.5	1.8	102.9	0.31	1.0	105	2.0
25	1.20	60	40	3.5	2	acetonitrile	0.45	0.111	92.2	0.4	158.7	0.29	0.5	64	1.1
26	1.65	60	40	5.0	1	acetonitrile	1.02	0.185	86.7	1.2	246.8	2.48	3.2	488	3.5
27	1.65	20	80	2.0	3	acetonitrile	1.04	0.353	73.2	8.3	288.7	51.91	44.8	6405	2.1
28	1.65	60	40	2.0	3	acetonitrile	0.87	0.189	85.8	0.9	301.5	3.11	4.6	692	1.9
29	0.75	60	40	2.0	3	acetonitrile	0.17	0.056	96.4	3.8	a	0.00	4.8E-3	0.8	3.8
30	1.65	40	60	3.5	2	acetonitrile	1.05	0.275	79.1	4.8	242.2	17.65	23.2	3641	1.2
31	0.75	60	40	2.0	1	acetone	0.44	0.066	95.5	5.3	76.9	0.01	0.06	15	0.79
32	1.65	20	80	5.0	1	acetone	1.60	0.482	69.2	11.7	215.1	157.59	71.00	13082	0.56
33	0.75	40	60	3.5	2	acetone	0.75	0.109	93.0	4.7	256.8	0.22	1.65	218	0.44
34	1.20	40	60	3.5	2	acetone	1.13	0.184	87.2	4.6	283.7	3.60	8.54	1117	0.36
35	1.20	40	60	3.5	2	acetone	1.13	0.189	86.8	5.6	297.0	3.44	6.86	1091	0.79
36	0.75	20	80	2.0	1	acetone	1.17	0.138	90.2	5.4	275.8	1.00	1.01	351	0.33
37	0.75	60	40	5.0	1	acetone	0.26	0.066	96.0	4.0	119.6	0.02	0.07	10	1.20
38	0.75	20	80	2.0	3	acetone	0.99	0.130	90.8	5.2	253.3	0.76	3.04	363	0.74
39	1.65	60	40	5.0	1	acetone	2.14	0.327	75.6	6.4	210.7	29.24	20.03	347	0.92
40	0.75	60	40	2.0	3	acetone	0.62	0.073	95.8	5.2	147.3	0.03	0.2	36	0.36

Table 4. Preparation conditions and measured properties for non-reinforced aerogels (Reprinted with permission from Publication 19. Copyright 2010 American Chemical Society).

Formulation #	Total Si, M	MTMS, mol%	BTMSPA, mol%	Water: Silane	Solvent	Bulk Density, g/cm^3	Porosity, %	Shrinkage,%	BET Surface Area m^2/g	Modulus, MPa	Max. Stress at Break, MPa	Toughness, kJ/m^3	Unrecovered strain, %
1	0.75	60	40	2.0	acetonitrile	0.055	96.3	5.1	a	a	a	a	a
2	1.20	40	60	3.5	acetonitrile	0.126	90.9	4.0	b	1.94	0.93	153	0.5
3	1.20	40	60	3.5	acetonitrile	0.124	91.9	3.2	394.9	1.93	0.75	115	1.1
4	1.65	20	80	5.0	acetonitrile	0.242	82.0	11.7	531.2	48.78	5.61	775	NA
5	0.75	20	80	5.0	acetonitrile	0.085	93.8	4.0	215.2	0.48	0.25	39	2.3
6	1.65	60	40	2.0	acetonitrile	0.147	89.0	3.0	b	2.87	0.46	50	NA
7	1.65	20	80	5.0	acetonitrile	0.234	82.6	10.1	521.0	38.05	5.39	745	0.9
8	1.20	40	60	5.0	acetonitrile	0.124	90.8	2.2	521.0	1.78	0.82	132	0.08
9	1.20	40	60	3.5	acetonitrile	0.124	90.7	4.0	531.2	1.44	0.96	160	0.44
10	1.20	40	60	2.0	acetonitrile	0.131	90.2	5.1	385.1	2.13	0.95	152	0.2
11	0.75	40	60	3.5	acetonitrile	0.067	95.1	0.6	215.4	a	a	a	a
12	1.20	40	60	3.5	acetonitrile	0.125	90.7	3.2	387.7	2.11	0.35	40	NA
13	1.20	20	80	3.5	acetonitrile	0.153	88.0	6.1	477.3	7.18	2.44	422	0.8
14	1.20	40	60	3.5	acetonitrile	0.127	90.6	4.3	371.1	2.11	0.54	76	1.2
15	1.20	40	60	3.5	acetonitrile	0.128	90.6	3. 7	393.8	2.34	0.87	148	1.5
16	0.75	20	80	2.0	acetonitrile	0.087	94.0	5.3	134.7	0.11	0.13	21	0.85
17	1.20	40	60	3.5	acetonitrile	0.124	90.7	3.5	b	2.13	1.06	175	1.1
18	1.20	40	60	3.5	acetonitrile	0.130	69.7	4.4	392.6	2.21	0.90	144	0.2
19	0.75	60	40	5.0	acetonitrile	0.052	96.7	5.3	a	a	a	a	a
20	1.65	20	80	2.0	acetonitrile	0.256	81.0	13.3	499.8	45.66	2.33	322	NA
21	0.75	60	40	5.0	acetonitrile	0.054	96.4	4.5	a	a	a	a	a
22	0.75	20	80	5.0	acetonitrile	0.086	94.1	3.9	b	0.45	0.26	43	1.0
23	1.65	60	40	5.0	acetonitrile	0.159	88.5	3.3	b	1.92	1.13	173	0.52
24	0.75	20	80	2.0	acetonitrile	0.093	93.1	5.1	122.2	0.31	0.48	73	0.1
25	1.20	60	40	3.5	acetonitrile	0.104	92.1	2.3	b	0.31	0.19	28	0.4
26	1.65	60	40	5.0	acetonitrile	0.155	88.4	3.8	412.5	2.14	0.99	148	0.6
27	1.65	20	80	2.0	acetonitrile	0.265	80.4	13.2	b	39.38	7.08	1171	1.4
28	1.65	60	40	2.0	acetonitrile	0.168	74.5	4.5	402.7	2.67	4.48	725	0.6
29	0.75	60	40	2.0	acetonitrile	0.055	96.3	5.1	a	a	a	a	a
30	1.65	40	60	3.5	acetonitrile	0.214	84.6	7.9	b	12.08	6.53	1126	1.3
31	0.75	60	40	2.0	acetone	0.061	96.45	9.2	179.9	0.02	0.10	9	0.00
32	1.65	20	80	5.0	acetone	0.287	80.34	14.7	589.6	41.23	12.72	2270	4.08
33	0.75	40	60	3.5	acetone	0.093	94.15	7.7	374.8	0.20	0.22	36	0.00
34	1.20	40	60	3.5	acetone	0.133	91.37	6.8	507.7	1.89	0.51	106	2.27
35	1.20	40	60	3.5	acetone	0.145	90.44	9.0	523.6	2.19	1.58	161	3.30
36	0.75	20	80	2.0	acetone	0.113	92.13	11.0	390.2	0.51	0.9	144	2.99
37	0.75	60	40	5.0	acetone	0.060	96.63	7.9	145.8	a	a	a	a
38	0.75	20	80	2.0	acetone	0.107	93.19	10.6	386.3	0.46	0.86	133	6.48
39	1.65	60	40	5.0	acetone	0.182	88.10	7.5	563.0	3.84	2.08	344	1.65
40	0.75	60	40	2.0	acetone	0.060	96.75	7.3	289.6	a	a	a	a

[a] Aerogels were not tested due their softness and/or fragility
[b] No samples available for testing.

Shown in Figure 6 are ^{13}C NMR spectra of formulations fabricated from different concentrations of total silicon and BTMSPA, and from both acetonitrile and acetone. Incorporation of Desmodur 3300A could be observed at about 148 ppm and 158 ppm (Figure 6 a-b) at highest concentration of total Si with highest concentration of BTMSPA. At the opposite end of the spectrum, there was little or no polymer present. These observations are in good agreement with results found in density.

As for mechanical properties, the increase in density leads to the increase in moduli, which holds true for both non-reinforced and reinforced aerogels. Again, an increase in modulus is also directly related to an increase in density or higher shrinkage (%), as well as in solvent, acetonitrile versus acetone. Shown in Figure 7 are typical stress-strain curves of non-cross-linked and cross-linked samples. The conformal coating of the polymer drastically improved not only the strength of the silica based aerogel, but also the unrecovered strain under repeated compression tests. Their improved flexibility and good recovery after 2 consecutive compressions at 25% strain compared to those non-cross-linked aerogel are listed in Tables 3 and 4, and are illustrated in Figure 8, where pairs of lines in the graphs represent two subsequent stress-strain curves.

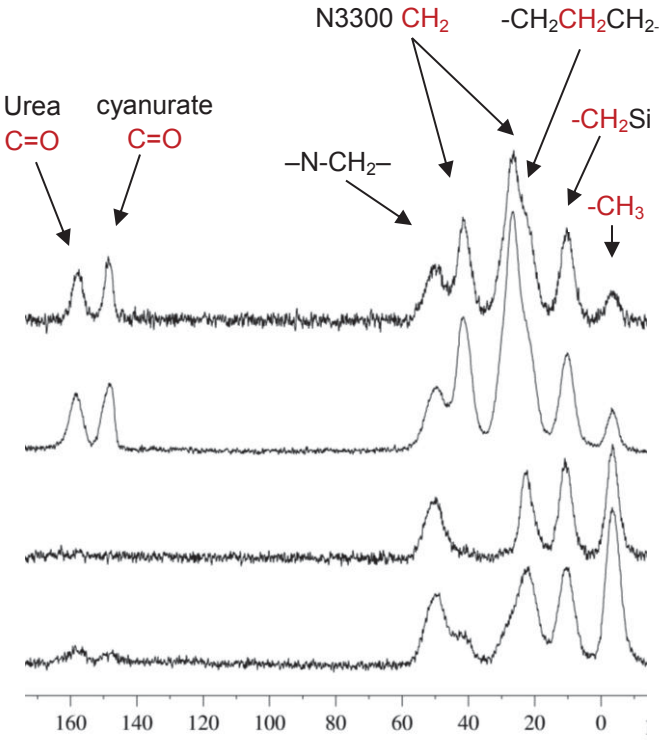

Figure 6. Solid ^{13}C NMR spectra of samples from formulations listed in Table 3. Sample spectra shown in a) acetonitrile and b) acetone were fabricated at highest Si concentration (1.65 mol/l) with 80 mol % BTMSPA derived Si, while c) acetonitrile and d) acetone were fabricated at lowest Si concentration (0.75 mol/l) Si with 40 mol % BTMSAP derived Si (Reprinted with permission from Publication 19. Copyright 2010 American Chemical Society).

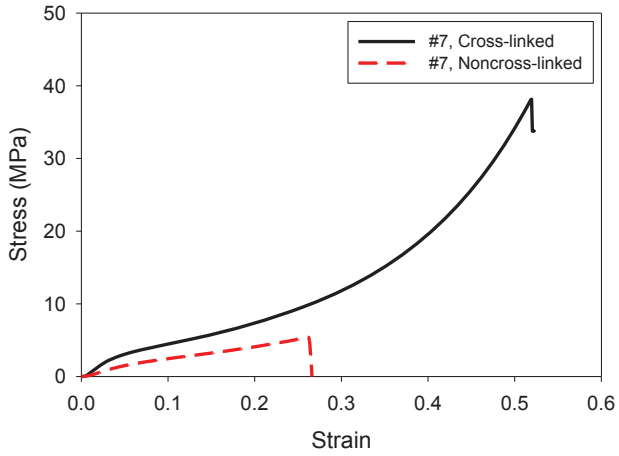

Figure 7. Typical stress-strain curves for a polymer reinforced aerogel compared to a non-reinforced aerogel, both prepared in acetonitrile (Reprinted with permission from Publication 19. Copyright 2010 American Chemical Society).

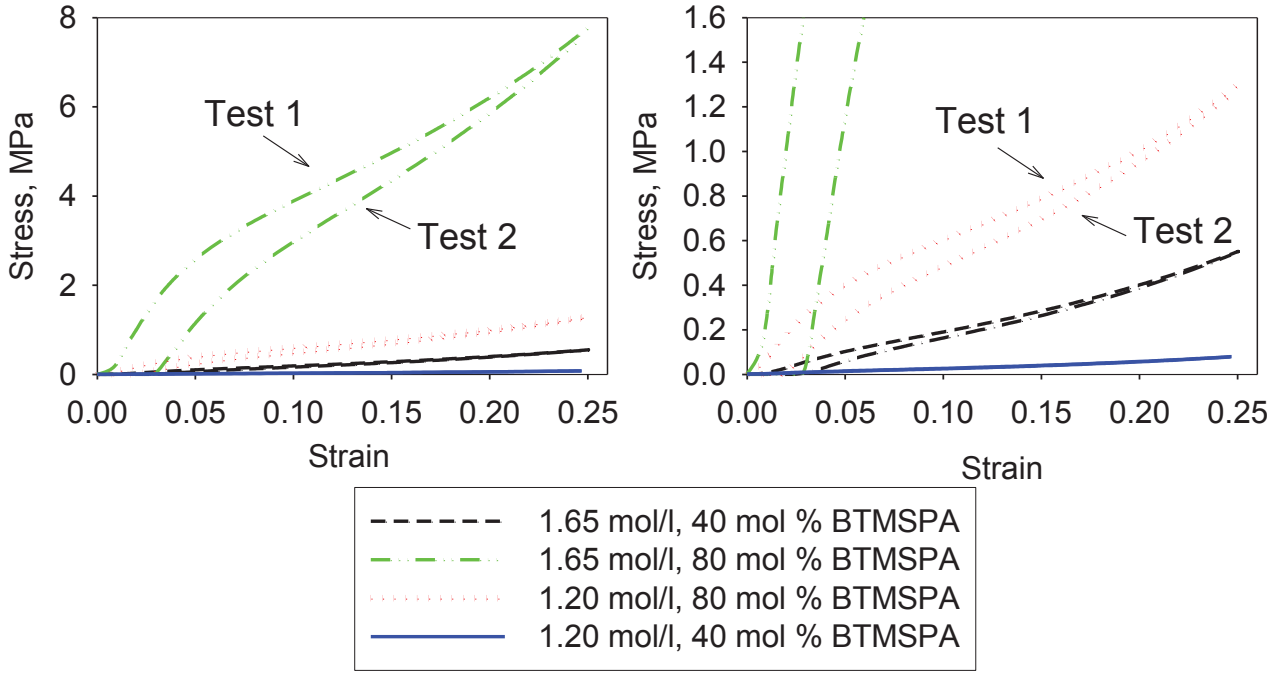

Figure 8. Typical stress-strain curves for a repeat compression tests on various polymer reinforced aerogels with different total silicon concentration and BMSPA levels of monoliths prepared in acetonitrile (Reprinted with permission from Publication 19. Copyright 2010 American Chemical Society).

2.2.3 Elastic Low Density Aerogels Derived from Bis[3-(Triethoxysilyl)propyl]disulfide, TMOS, and Vinyl trimethoxysilane by two-step process (Publication 24)

In this study, we combined bridged silsesquioxane, Bis[3-(Triethoxysilyl)propyl]disulfide (BTSPD), and a trialkoxysilane, VTMS to further improve the flexibility and elastic recovery of silica based aerogels. BTSPD comprised of two propyl units linked by a sulfur-sulfur bond, provides a flexible bridging group in the silica structure as shown in Scheme 6. VTMS, with a hydrophobic vinyl group is similar to MTMS in that only three Si-O bonds are possible for the hydrolysis and condensation reactions to take place. In addition, vinyl, being larger than the methyl group, may alter the pore structure, as well as provide a reactive site for polymer reinforcement. Reinforcing the aerogel structure by co-reacting styrene or other -ene moieties with the surface vinyl groups supplied by VTMS may provide even higher strengths, analogous to other polymer reinforced aerogels. As shown in Scheme 6, VTMS and BTSPD are copolymerized with TMOS using a two-step (acid-base) sol-gel synthesis, and ethanol as a solvent. The goal of the research is to produce aerogels with a combination of high strength, high surface area, and good elastic recovery. Such a robust aerogel may be enabling for aerospace applications such as for space suits for Mars surface missions where a combination of the best thermal insulation and robust mechanical properties is needed.

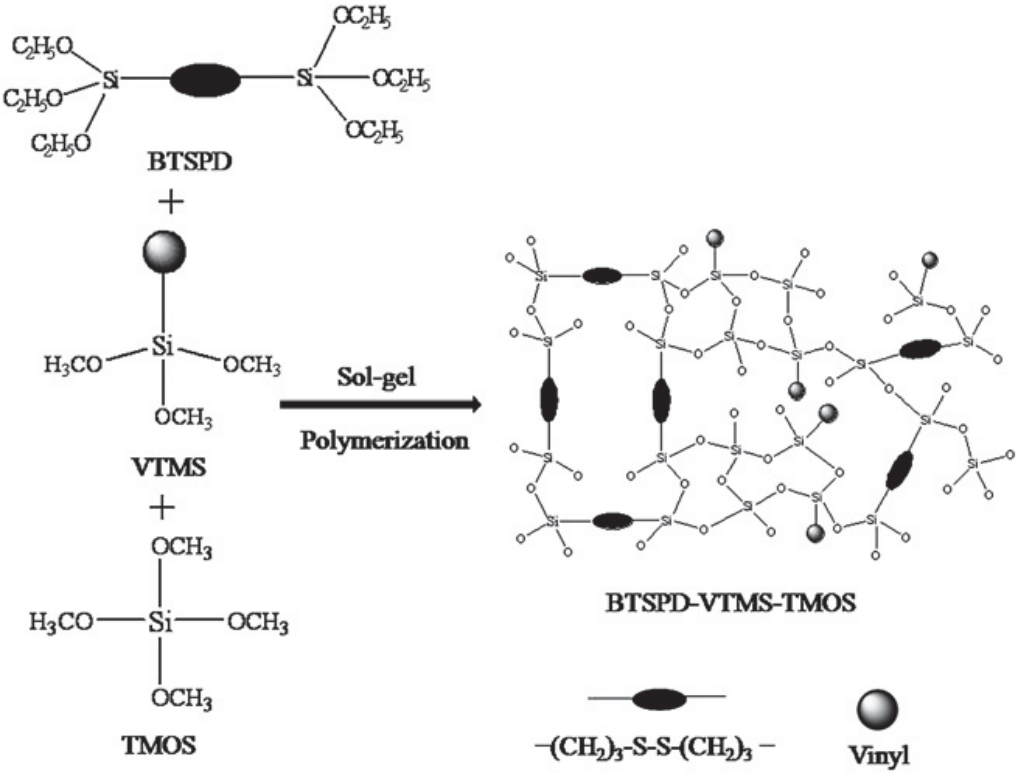

Scheme 6. Formation of network using BTSPD, TMOS, and VTMS in a sol-gel process. (Reproduced from Publication 24 with the permission from The Royal Society of Chemistry.)

Statistical experimental design methodology is applied to examine the effects of three variables, the concentrations of BTSPD, VTMS, and TMOS on the structure and properties of the resulting samples. The total molar ratio of the nitric acid to total Si was fixed at 0.49:1 and a volume ratio of 2M nitric acid to 28% NH_4OH of 1:2 was used. Preliminary work found that sturdy gels were formed only when the acid to base volume ratio is 1:2. At higher ratio of acid

to base, gelation did not take place, while at lower ratio, settling of particles was observed. Monoliths were made using concentrations of VTMS and BTSPD varied from 0.1 to 0.3 mol/l and TMOS varied from 0.1 to 0.5. Combinations of 0.1 mol/l BTSPD and 0.1 mol/l TMOS with 0.1 and 0.2 mol/l VTMS did not gel. In addition, samples from the formulation labelled as 19 in Table 5 using the same amount of BTSPD and TMOS with 0.3 mol/l VTMS were too fragile for compression testing and contact angle measurements.

The properties of the aerogels are shown in Table 5. All samples produced were white and opaque, as shown in Figure 9. Shrinkage occurring over the entire fabrication process, measured as the difference between the diameter of the mold and the dried monolith was fairly uniform across the study, ranging between 10 to 20 %.

Table 5. Preparation conditions and measure properties of monoliths made from BTSPD, TMOS, and VTMS[a]. (Reproduced from Publication 24 with the permission from The Royal Society of Chemistry.)

#	VTMS (mol/l)	BTSPD (mol/l)	TMOS (mol/l)	Density (g/cm^3)	Porosity %	Modulus (MPa)	Unrecovered strain, %	Surface Area (m^2/g)	Contact Angle (^{o})
1	0.1	0.1	0.5	0.126	91.6	0.50	11.9	656	129
2	0.2	0.1	0.5	0.137	90.6	0.72	8.05	718	129
3	0.3	0.1	0.5	0.185	87.7	2.29	1.2	598	132
4	0.1	0.2	0.5	0.153	89.6	1.35	1.2	461	130
5	0.2	0.2	0.5	0.170	88.7	1.36	1.3	416	137
6	0.3	0.2	0.5	0.194	86.6	1.78	1.7	439	137
7	0.1	0.3	0.5	0.212	85.8	3.72	1	308	137
8	0.2	0.3	0.5	0.248	83.2	3.16	1.6	295	141
9	0.3	0.3	0.5	0.257	82.4	4.65	1.2	347	143
10	0.1	0.1	0.25	0.088	93.5	0.03	9.1	218	122
11	0.2	0.1	0.25	0.115	91.8	0.12	4.2	240	128
12	0.3	0.1	0.25	0.142	89.7	0.30	4.3	276	135
13	0.1	0.2	0.25	0.118	91.5	0.24	0.8	48.7	134
14	0.2	0.2	0.25	0.140	89.7	0.46	1.7	68.2	135
15	0.3	0.2	0.25	0.180	87.0	0.86	0.7	97.2	135
16	0.1	0.3	0.25	0.163	88.1	0.99	1.3	95.0	131
17	0.2	0.3	0.25	0.182	86.7	2.28	0.9	100	136
18	0.3	0.3	0.25	0.227	83.5	3.71	1	139	138
19	0.3	0.1	0.1	0.067	94.8	b	b	3.42	b
20	0.1	0.2	0.1	0.091	93.3	0.01	0(75%)	6.56	125
21	0.2	0.2	0.1	0.097	93.0	0.06	0.2	20.8	129
22	0.3	0.2	0.1	0.117	91.5	0.19	0.2	34.6	143
23	0.1	0.3	0.1	0.187	86.5	0.36	1.2	51.4	133
24	0.2	0.3	0.1	0.167	87.2	0.92	2.5	64.6	134
25	0.3	0.3	0.1	0.189	86.0	2.07	2.8	69.6	143

[a] Combinations of 0.1 mol/l and 0.2 mol/l VTMS, with 0.1 BTSPD and 0.1 mol/l TMOS did not gel and thus are not reported.

[b] Formulation too fragile to test

Figure 9. Photos of the selected samples made with BTSPD, TMOS, and VTMS. (Reproduced from Publication 24 with the permission from The Royal Society of Chemistry.)

The bulk density of the samples in the study ranged from 0.070 to 0.257 g/cm^3. Density increased with increasing concentrations of VTMS, BTSPD, and TMOS. Increasing silane concentration in general increases the amount of silica in the sample while increasing VTMS and BTSPD also causes an increase in the amount of organic pendant or bridging groups in the samples. BTSPD concentration has the largest effect on density because it contains the largest bridging organic group and contributes two Si groups. The porosities of the samples range from 82 % to 95 %. Porosity decreases with increasing amounts of silane precursors, in opposition to density (the more solid phase, the less porosity.) BTSPD again has the largest effect by contributing both increased amounts of Si and organic to the monoliths.

The adsorption isotherms of the samples are an IUPAC type IV curve with an H1 hysteresis loop, indicating that the monoliths consist predominately of three dimensional continuous meso-macropores. When the total silane amount of BTSPD and VTMS is greater than that of TMOS (as in sample 23), plateaus at high relative pressure (P/P_0) were observed, indicating the modification of the pore structures of the organic groups derived from BTSPD and VTMS. Samples with extremely low surface area, such as samples 19 and 20, no adsorption and desorption isotherm curves can be obtained, indicating loss of mesoporosity.

The surface areas range from 3 m^2/g to as much as 720 m^2/g as seen in Figure 10. Increasing TMOS concentration significantly increases surface area. However, increasing BTSPD, especially when TMOS concentration is high, causes a decrease in surface area. In fact, when TMOS concentration is at 0.5 mol/l, surface areas drop by half going from low to high BTSPD concentrations (350 m^2/g to 700 m^2/g). At 0.1 mol/l TMOS, BTSPD concentration has less of an effect on surface areas. In these cases, all surface areas were small, ranging from 3 m^2/g to 70 m^2/g for all the samples., Again, note that at the lowest levels of TMOS and BTSPD, only the formulation with VTMS at 0.3 mol/l was able to be produced. VTMS has no significant effect on surface area.

The difference in nanostructure can also be seen from SEM images as shown in Figure 11. For the aerogels made using high concentrations of TMOS (0.5/mol/l), higher BTSPD concentration leads to larger particle sizes and larger pores. Hence, the surface area is decreased. Samples 4 (Figure 11a) and 7 (Figure 11b) both produced using 0.5 mol/l of TMOS, show a typical aerogel morphology with a fine distribution of uniformly small particles. However, the pore structure of the monoliths made using 0.2 mol/l BTSPD (Figure 11a) and that made using 0.3 mol/l BTSPD (Figure 11b) have a wide distribution of pore sizes ranging from 10 nm to 200 nm. This effect on pore structure due to incorporating an organic linking group into the silica backbone is again the same as that observed with increasing BTMSH in the epoxy reinforced aerogels previously studied. Decreasing the concentration of TMOS to 0.1 mol/l leads to larger pore diameters as seen in the micrographs of sample 20 (Figure 11c) and

sample 23 (Figure 11d). However, at the lowest TMOS concentration, when decreasing BTSPD amount from 0.3mol/l to 0.2 mol/l, the particle size increases from 50nm (Figure 11d) to 1-2.5μm (Figure 11c). Note that these micrographs are shown at a different scale.

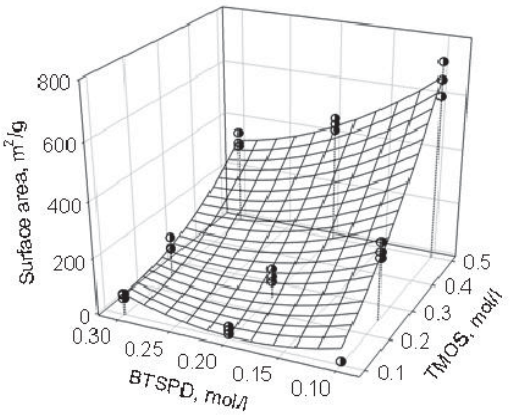

Figure 10. Graph of empirical model for surface area vs. BTSPD and TMOS concentration shown with raw data. Note that VTMS is not a significant factor in the model over and above random error. (Reproduced from Publication 24 with the permission from The Royal Society of Chemistry.)

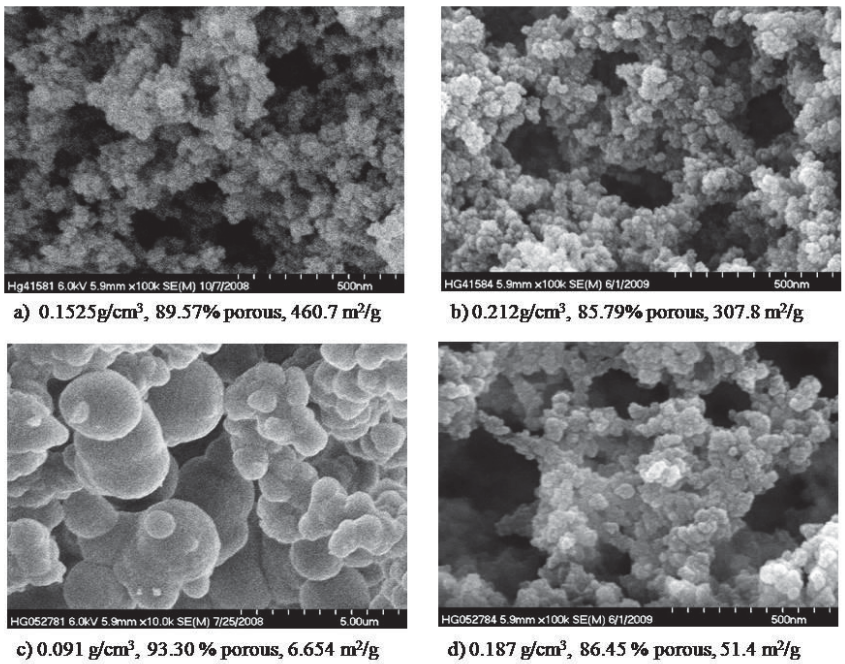

Figure 11. SEM images of a) sample 4 (0.2 mol/l BTSPD) and b) sample 7 (0.3 mol/l BTSDP) made using 0.5 mol/l TMOS, compared to samples made with 0.1 mol/l TMOS c) sample 20 (0.2 mol/l BTSPD) and d) sample 23 (0.3 mol/l BTSPD). (Reproduced from Publication 24 with the permission from The Royal Society of Chemistry.)

Decreasing the amount of TMOS not only causes a difference in the nanostructure (surface area, pore size, and morphology) but may attribute to the solubility differences of the siloxy

precursors in the ethanol/water mixture used to produce the gels. When more TMOS is used, ethanol solvates the siloxy groups leading to a well dispersed array of small particles and pores. The aliphatic groups are not as soluble in the aqueous ethanol, resulting in more phase separation in the gel, larger particle sizes and a collapse of the mesoporosity.

All samples are relatively hydrophobic with contact angles of at least 120°. As seen from Figure 12, hydrophobicity increases with increasing BTSPD, TMOS, and VTMS concentration, with the greatest effect if VTMS covers the silica surface with hydrophobic vinyl groups. At high VTMS concentration, TMOS concentration has no effect on measured contact angles. At low VTMS, decreasing TMOS concentration decreases the contact angle. The highest contact angles measured in the study (143°) are for samples containing the highest levels of BTSPD and VTMS, regardless of TMOS concentration.

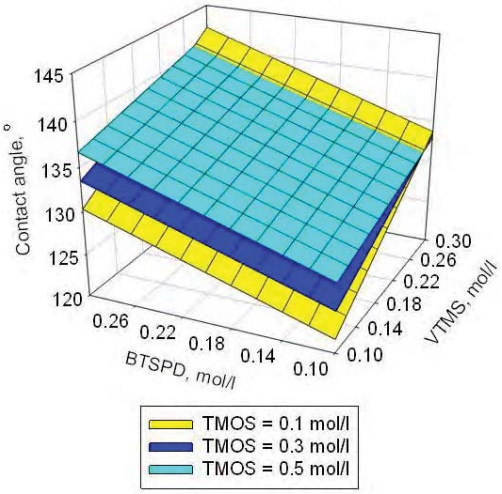

Figure 12. Graph of empirical model for water contact angle vs. BTSPD and VTMS concentration at three levels of TMOS concentration. (Reproduced from Publication 24 with the permission from The Royal Society of Chemistry.)

Compression tests were run on all monoliths from Table 5, except sample 19, since this formulation was very fragile. As shown in Figure 13a, TMOS concentration has the largest effect on modulus, with modulus increasing with increasing TMOS concentration. At high TMOS concentration, the response surface is very flat, which indicates that there is no significant effect of VTMS or BTSPD concentration on modulus. At lower concentrations of TMOS, modulus is seen to increase with increasing BTSPD and VTMS concentration, in response to a greater change in density over the range of samples.

The power law relationship between density and modulus is graphed in Figure 13b. A greater increase in the exponent compared to the native silica aerogels (TMOS or TEOS alone) was noted, which is similar to that reported for styrene reinforced aerogels derived from TMOS, VTMS, and BTMSH. Power law relationships between modulus and density for native silica aerogel are typically reported with an exponent of 3 to 3.7 depending of the synthesis route and have been shown to depend predominantly on the connectivity between particles. The greater increase in the exponent for the aerogels is most likely due to molecular structure variations of TMOS, VTMS and BTSPD causing differences in the skeletal structures that are observed by SEM.

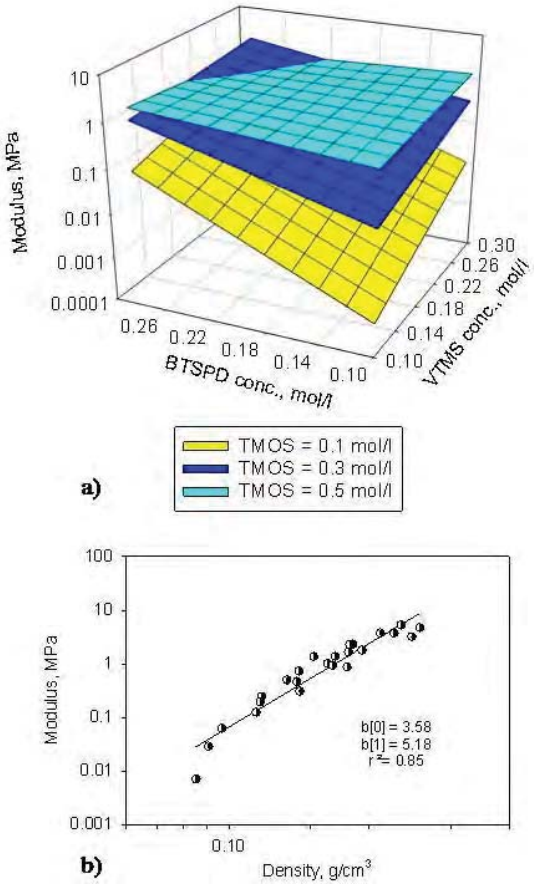

Figure 13. Graph of a) empirical model for compressive modulus vs. BTSPD and VTMS concentration and b) power law relationship between density and modulus. (Reproduced from Publication 24 with the permission from The Royal Society of Chemistry.)

All of the monoliths in the study with BTSPD concentration of at least 0.2 mol/l exhibit low unrecovered strain (or high elastic recovery). The sample made using 0.1 mol/1 TMOS, 0.2 mol/l BTSPD, and 0.1 mol/l VTMS recovers most completely even after compressing to 75 % strain as illustrated in the stress strain curve in Figure 14a. Figure 14b shows sample 20 before, during, and after compressing the sample with finger pressure. As seen in Figure 14c, sample 20 recovers 98% of their original length during the first ten minutes after compression and 99.6% after thirty minutes.

Figure 15 demonstrates that BTSPD concentration is the most important factor on elastic recovery. Unrecovered strain significantly decreases with increasing BTSPD concentration, reaching a highest recovery at about 0.21-0.25 mol/l BTSPD depending on TMOS concentration. Increasing TMOS concentration slightly increases unrecovered strain, when BTSPD concentration is lower. Since VTMS has a similar structure to MTMS (three siloxy bonding sites and an unreactive aliphatic group, it is expected that increasing VTMS concentration also decreases unrecovered strain (increases recovery) as MTMS derived aerogel when BTSPD concentration is low. However, surprisingly, increasing VTMS concentration does not improve elastic recovery when BTSPD is at a higher concentration.

Therefore, we can conclude that including bis(alkoxysilanes) linked with organic groups is a more effective way to introduce elastic recovery to the aerogels.

At the optimum BTSPD concentration, elastic recovery is good (unrecovered strain is low) for all levels of TMOS concentration. This is an important finding since there is a trade off in some properties when using BTSPD (e.g., extremely low BET surface areas which are a strong predictor for insulation quality). However, good recovery in formulations with both high TMOS concentration and optimum BTSPD means that it is possible to make stronger aerogels with a combination of higher modulus, good recovery, high BET surface areas and good hydrophobicity. In fact, as predicted by the model, a combination of 0.5 mol/l TMOS, 0.3 mol/l VTMS concentration, and 0.22 mol/l BTSPD should lead to optimized aerogels with a density of 0.21 g/cm^3, porosity of 85.5%, Young's modulus of 2.1 MPa, a water contact angle of 138 ^{o} and near complete recovery after compression (1.3 % unrecovered strain). Using this combination of silanes, an authentic aerogel sample was synthesized and measured to have density 0.20 g/cm^3, porosity of 85.3%, Young's modulus of 2.4 MPa, 1.4 % unrecovered strain after compression to 25 % strain, and water contact angle of 142 ^{o}; all are in good agreement with the model prediction.

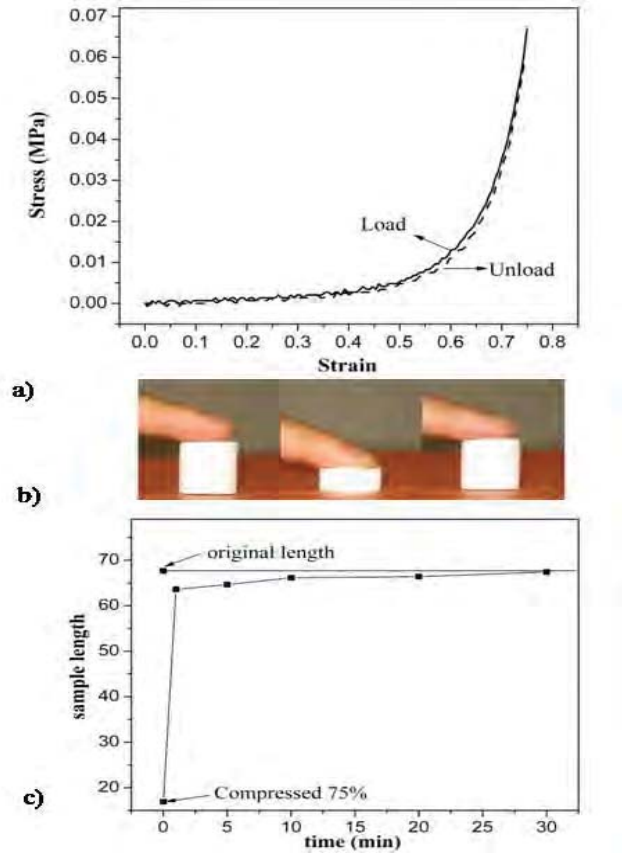

Figure 14. a) Stress strain curves of sample 20 from Table 5 compressed to 75% strain twice. (Solid line: first compression; dashed line: second compression.), b) sample 20 compressed by finger pressure demonstrating full recovery, and c) recovery after compression of sample 20 vs. time. (Reproduced from Publication 24 with the permission from The Royal Society of Chemistry.)

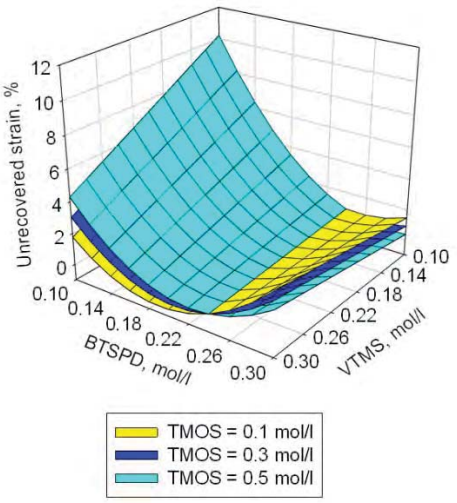

Figure 15. Graph of empirical model for unrecovered strain vs. BTSPD and VTMS concentration. (Reproduced from Publication 24 with the permission from The Royal Society of Chemistry.)

3. Synthesis, Characterization, and Processing of Low Density, Flexible and Cross-linked Polyimide Aerogels (Publications 4-7, 9-11,13, 15-16)

While polymer reinforced silica-based aerogels exhibit a great improvement in strength over their native silica counterparts, for many applications it is desirable to have a more flexible or elastic material. For example, insulation for extravehicular activity (*EVA)* suits should also be durable and flexible to accommodate as much freedom of movement for the astronaut as possible. Another use for flexible, durable aerogels could be as part of an inflatable decelerator used to slow spacecraft for planetary entry, descent, and landing (*EDL*). *EDL* systems used to successfully land six robotic missions on Mars from 1976 to 2008 employed a hard aeroshell heat shield and parachutes of 12-16 m in diameter. Future robotic and manned missions are much heavier and will require more drag for landing. Hence, new designs with much larger diameters (30-60 m) will be required. Inflatable decelerators would stow in a small space and deploy into a large area lightweight heat shield to survive reentry. Minimizing weight and thickness of the system as well as providing suitable insulation are important considerations.

Previously reported linear polyimide aerogels produced at Aspen Aerogel exhibited large shrinkage. A swelling problem was also observed when some cross-linked amic-acid sol-gels were imidized at high temperature. To overcome these defects, multifunctional amine moieties such as octa(aminophenyl)silsesquioxane (OAPS) or 1,3,5-triaminophenoxybenzene (TAB) have been employed to build a more stable 3-D network. OAPS is a nanoscale polyhedral oligomeric silsesquioxane cage structure consisting of a silicon and oxygen framework with eight aminophenyl groups attached. Such polyhedral oligomeric silsesquioxane cage structures with various reactive groups can be incorporated into polymers to improve thermal and mechanical properties, dielectric properties, atomic oxygen resistance and abrasion resistance. TAB, with its tri-functional reactive sites, also form a network structure that can result in strong, yet flexible aerogels that films can be cast, having many potential application both for space and industrial uses. Another study in which an addition aromatic di-isocyanate, 4,4'-methylene di-isocyanate (MDI), in combination with TAB, has also been used as a cross-linker to form a 3-D polyimide/polyurea (PI-PU) block co-polymer aerogels. Different synthetic methods including

thermal imidization at low temperature (110°C) using 1,4-diazobicyclo[2.2.2]octane (or DABCO) as catalyst have also been examined. However, chemical imidization, using of both acetic anhydride and pyridine as catalysts, has shown to be the most feasible route in processing.

Compared to polymer reinforced silica-based aerogels, these new types of materials have lower density, lower shrinkage, higher modulus, and comparable thermal conductivity (14 mW/m-K for aerogels with density of 0.1 g/cm^3) to silica aerogel. These flexible, thin aerogel films are stable up to 400^{o}C for a short term exposure.

3.1. OAPS Cross-linked Polyimide Aerogels (Publications 6 and 9)

OAPS is a nanoscale polyhedral oligomeric silsesquioxane cage structure consisting of a silicon and oxygen framework with eight aminophenyl groups attached. Polyimide nanocomposites fabricated from OAPS show enhancements in thermal and mechanical properties. In this study, as shown in Scheme 7, OAPS is used to form a cross-linked poly(amic acid) by reacting with the terminal anhydride groups of oligomers made from dianhydride and diamines in N-methylpyrolidinone (NMP). A variety of dianhydrides and diamines can be used. For example, the dianhydride can be selected from the group consisting of benzophenone-3,3',4,4'-tetracarboxylic dianhydride ("BTDA") and biphenyl-3,3',4,4'-tetracarboxylic dianhydride ("BPDA"). Also for example, the diamine can be selected from the group consisting of 3,4-oxydianiline ("3,4-ODA"), 4,4'-oxydianiline ("4,4'-ODA" or "ODA"), *p*-phenylene diamine ("PPDA"), 2,2'-dimethylbenzidine ("DMBZ"), and bisaniline-*p*-xylidene ("BAX"). The dianhydride and/or diamine can be selected based on being commercially available or being known to impart different properties to polyimides in general. BPDA, PPDA, and DMBZ are known to produce a rigid backbone in polyimide structures, while ODA and BTDA have flexible linking groups between phenyl rings resulting in flexible structures. Both molded cylinders and thin flexible films have been made.

A typical procedure in making these cross-linked polyimide aerogel involves the reaction of the terminal anhydride groups from the polyamic acid oligomers with the amines of OAPS, after which acetic anhydride (to scavenge water bi-product of condensation), and pyridine (to catalyze imidization) are added to the solution. Gelation varies with the different polyimide oligomers. Figure 16 shows a NASA logo made with OAPS cross-linked polyimide aerogel using BPDA, and DMBZ. The color and transparency of the polyimide aerogel films depends on the backbone structure of the polyimide oligomers. For example, OAPS cross-linked polyimide aerogel film is opaque yellowish if using BAX, but transparent if ODA, DMBZ (yellowish) or PPDA (dark orange) is used.

The final properties, such as density, porosity, shrinkage surface area, and Young's modulus were dependent on the backbone chemistry. Stiffness and planarity of backbone and interaction with solvent during gelation leads to different amounts of shrinkage and therefore density. For the same dianhydride and diamine combination, number of repeat unit n does not affect the density and porosity. In all aerogels made from 10wt% total precursor solutions and using BPDA as dianhydride, the density of the aerogel samples range from 0.09 g/cm^3 to 0.3 g/cm^3. Porosity of polyimide aerogels ranges from 84% to 94%. Surface area ranges from ~250 m^2/g to ~507 m^2/g. PPDA polyimide-aerogel has the highest density, lowest porosity, and highest shrinkage (40%). DMBZ polyimide-aerogel (stiff, non-coplane backbone) has the lowest density, highest porosity, lowest shrinkage (6%), and the highest surface area (507 m^2/g).

Figure 16. A OAPS cross-linked polyimide aerogel sample made with BPDA and DMBZ.

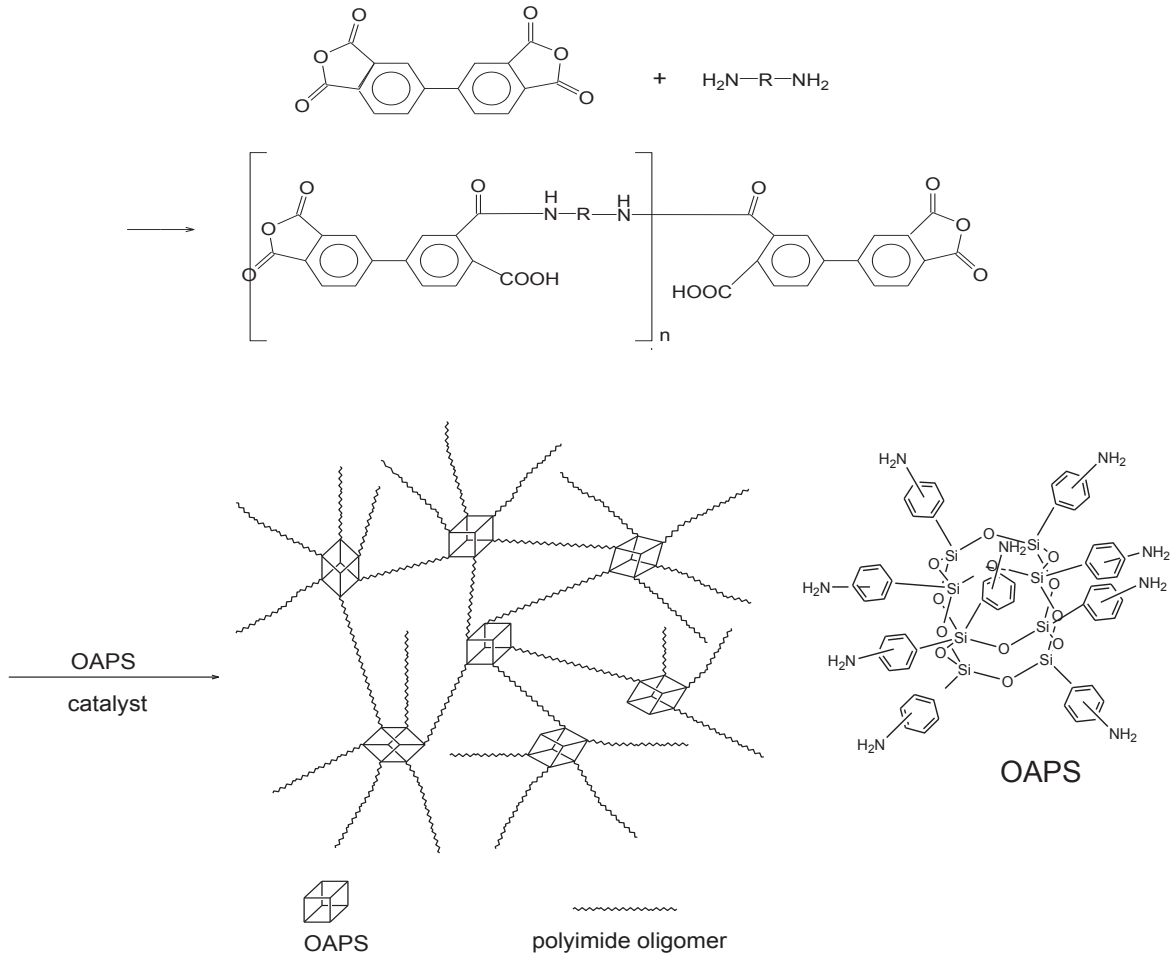

Scheme 7. The synthesis of the OAPS cross-linked polyimide aerogel network, where n is the repeating unit (Reprinted with permission from Publications 6 and 9. Copyrights 2012 and 2011 American Chemical Society, respectively).

The polyimide aerogels have modulus as high as or higher than previously reported polymer reinforced silica aerogels. At n=25, polyimide aerogel made with PPDA (stiff, planar backbone) has the highest young's modulus, about 67 Mpa and BAX polyimide aerogel has the lowest young's modulus. Generally in aerogels, the modulus increases as density increases. Aerogels made using PPDA follow this same trend, with modulus and density both increasing with increasing PPDA content. Surprisingly, Young's modulus of aerogels made using DMBZ increases slightly with increasing DMBZ content, while the density as previously mentioned actually decreases slightly. It is possible to fabricate a polyimide aerogel with both low density and high modulus by increasing the ratio of DMBZ in the aerogel structure.

SEM images of the selected polyimide aerogel formulations made in molded cylinder form are shown in Figure 17 (a-d). Unlike silica aerogels, the polyimide aerogels consist of a three dimensional network of polyimide nanofibers tangled together with fiber diameters ranging from 15 nm to 50 nm. The nanofiber structure possibly forms during polymerization and subsequent gelation with influence from solvent interaction. Polyimide aerogel made using PPDA as the diamine has densely packed strands (Figure 17b), which may be due to the greater chain rigidity, high planarity, and shorter chain length between cross-links of the polyimide oligomers, leading to greater shrinkage during processing, while polyimide aerogels made using BAX (Figure 17a), ODA (Figure 17c), and DMBZ (Figure 17d) have more open porosity around the fiber strands.

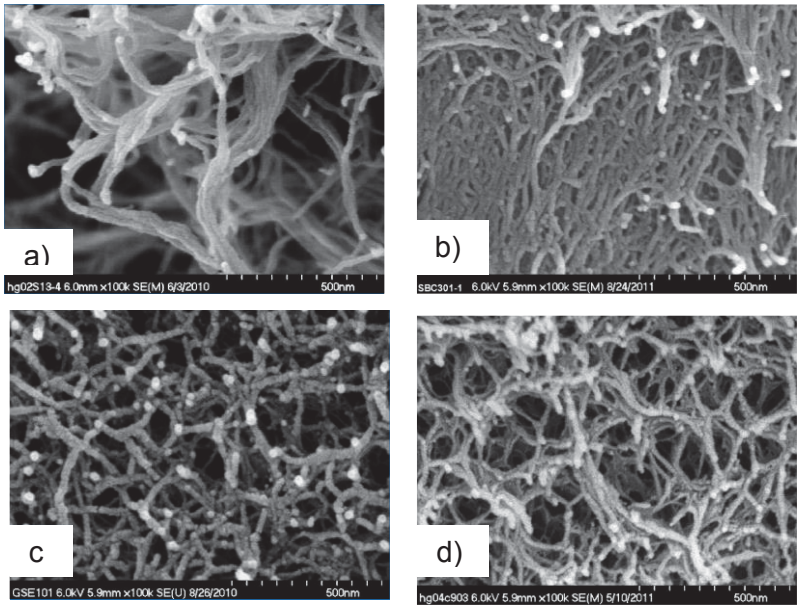

Figure 17. SEM images of polyimide-aerogels from (a) BAX, (b) PPDA, (c) ODA, and (d) DMBZ (Reprinted with permission from Publications 6 and 9. Copyrights 2012 and 2011 American Chemical Society, respectively).

With onset temperature of decomposition (T_d) of 560°C-630°C, the aerogels are quite stable, losing only 1-2 % weight on aging for 24 hours at 300 and 400 °C, suggesting short term use at these temperatures is possible. Polyimide aerogel made with BAX (flexible backbone) has the lowest T_d, and loses the most weight after heat treatment at 500°C. PPDA polyimide aerogel has the highest T_d and the least weight loss after heat treatment at 500 °C. All have high char-yield and T_d above 600 °C at high heating rate. As seen Figure 18, SEM images of OAPS

cross-linked polyimide aerogel made with BPDA and BAX after heating at 300 °C and 400 °C show little change. After 24 hours at 500°C, however, weight loss is 22.4% and as shown in Figure 18d, the mesoporous structure has collapsed.

As seen in Figure 19, at room temperature, the polyimide aerogels made with BAX (14.4 mW/mK, 760 torr) and ODA (20 mW/mK, 760 torr) have thermal conductivity similar to silica aerogels of the same density. The thermal conductivities also increase with increasing temperature as expected and drop at vacuum, which are also similar to that of the silica aerogels. The thermal conductivity of polyimide aerogel with BAX drops to 4.3 mW/m-K at 0.01torr, and drops to 6.54 mW/m-k at $1x10^{-5}$ torr using ODA. Because reducing the pressure lengthens the mean free path of the gas relative to the mean pore diameter, thermal diffusivity drops and thus so does the thermal conductivity.

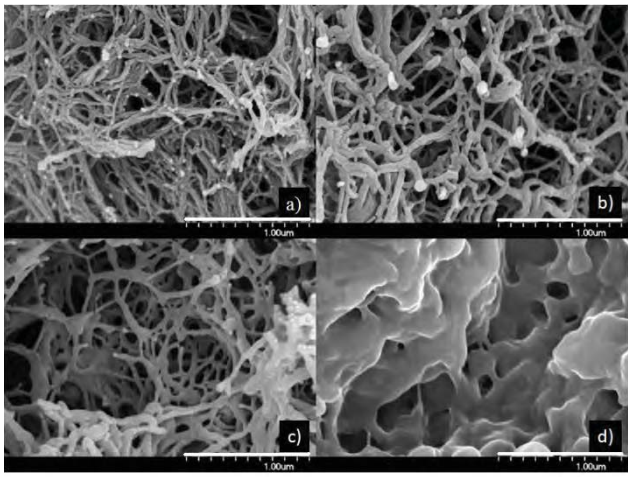

Figure 18. SEM images of the OAPS cross-linked polyimide aerogel (n = 20) at a) room temperature and after heating for 24 hours in nitrogen at b) 300 °C, c) 400 °C, and d) 500 °C. The scale bars in the micrographs are all 1.00 μm. (Reprinted with permission from Publication 9. Copyrights 2011 American Chemical Society).

Two or more dianhydrides and/or diamines combination can also be used to tailor properties of the resulting cross-linked polyimide aerogels. For example, a diamine like PPDA or DMBZ, having a rigid polyimide backbone, can be combined with a diamine, such as ODA, having flexible linking groups between phenyl rings. As seen in Table 6, PPDA or DMBZ and ODA can be used in combination with the mole percent of PPDA, or DMBZ varied from 0 mol% to 100 mol% of the total diamine, and ODA from 100 mol% to 0 mol%.

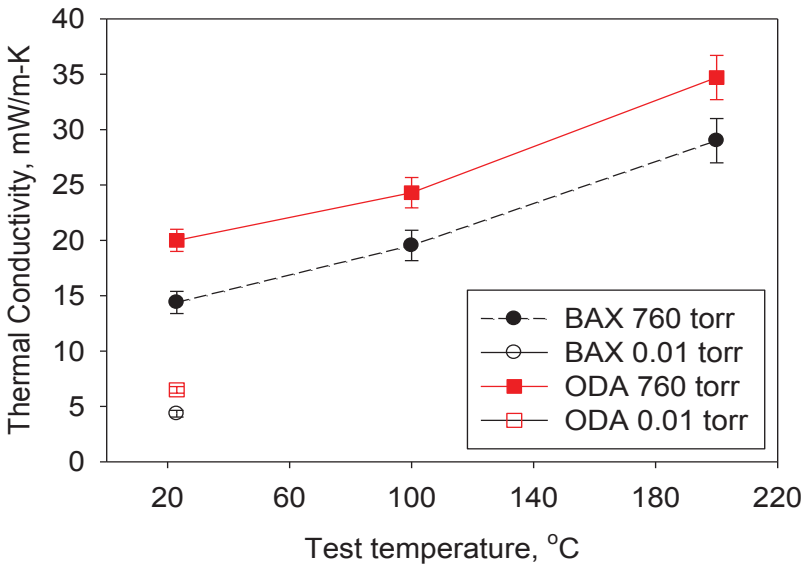

Figure 19. Thermal conductivities of OAPS cross-linked polyimide aerogels made with BAX and ODA (Reprinted with permission from Publication 9. Copyrights 2011 American Chemical Society).

Large Scale Fabrication: In collaboration with the University of Akron, highly flexible, thin polyimide aerogel films have been fabricated on a large scale, 1 ft. wide and up to 8 ft. long, versus the lab scale of 3"x8". Physical, thermal and mechanical properties, as well as morphology of aerogel monoliths and aerogel films have been analyzed. Figure 20 shows the casting of the polyimide aerogel film with a casting speed of 80 cm/min and a 12" wide Dr. Blade with a gap of 1.09 mm. The dry films have a thickness of nominally 0.3 to 0.7 mm. The properties of the polyimide aerogel films made with combination of DMBZ and ODA are listed in Table 6. Figure 21 shows a SEM image of a cross-section of a polyimide aerogel film made using a 50/50 mol% mixture of DMBZ and ODA. The surface of the film appears denser which may due to the solvent evaporation in the casting process, but the interior of the film has a fiber-like structure similar to the thicker cylindrical samples.

Films from all formulations were soaked in water for 24 hours and later dried in air to test moisture resistance. Aerogels made with BPDA and at least 50 mol% DMBZ or 100 mol% BAX were water resistant. As shown in Figure 22, 50 mol% DMBZ aerogel remained floating on the surface of the water, but a sample made using 100 mol% ODA absorbed water into the pores and sank to the bottom after a short time. Those aerogels which absorbed water tended to shrivel on air drying. The aerogels made with at least 50 mol% DMBZ were unchanged drying in air. Water contact angle measurements of these polyimide aerogel films made with 50-100 mol% DMBZ range from 85° to 90°. Films fabricated with 100 mol% DMBZ are the most brittle among all the films while formulations made using at least 50 mol% ODA are quite flexible. The thin polyimide aerogel film made using 50 mol% DMBZ (Figure 22) maintains the flexibility to bend back nearly 180° without cracking or flaking after being soaked in water and dried in air.

Table 6. Process variables and properties of polyimide aerogels prepared in the study. Note that ODA fraction is (100 mol% – rigid diamine mol%) (Reprinted with permission from Publication 6. Copyrights 2012 American Chemical Society).

Rigid diamine, %	Rigid diamine type	Density (g/cm^3)	Film density (g/cm^3)	Surface area (m^2/g)	Porosity (%)	Shrinkage (%)	Young's modulus (Mpa)	Tensile modulus, (MPa)	Tensile stress at break, MPa
100	PPDA	0.296	0.395	380	82.0	38.3	78.7	167.5	4.5
75	PPDA	0.267	0.400	362	83.4	36.4	54.3	155.0	3.9
50	PPDA	0.291	0.451	325	80.3	37.7	51.7	130.9	3.5
25	PPDA	0.206	0.274	335	85.8	29.5	20.2	72.2	1.6
0	PPDA	0.122	0.163	254	91.4	16.2	18.4	35.2	2.1
100	DMBZ	0.086	0.108	507	94.1	6.0	17.9	72.8	2.1
75	DMBZ	0.086	0.150	404	93.8	6.1	25.6	76.6	1.9
50	DMBZ	0.094	0.197	434	93.8	8.5	21.5	58.6	3.4
25	DMBZ	0.101	0.132	371	93.1	9.8	18.0	40.0	1.2
0	DMBZ	0.116	0.162	270	92.4	14.1	10.4	25.4	1.4
100	PPDA	0.268		413	85.3	36.9	56.0		
50	PPDA	0.214		385	86.2	31.2	26.7		
0	PPDA	0.133	0.166	292	91.4	19.0	23.9	33.7	1.2
100	DMBZ	0.089		489	93.9	6.7	22.1		
50	DMBZ	0.110	0.179	351	92.8	12.9	18.5	54.8	1.8
0	DMBZ	0.153	0.157	366	90.7	19.7	19.4	31.2	1.3

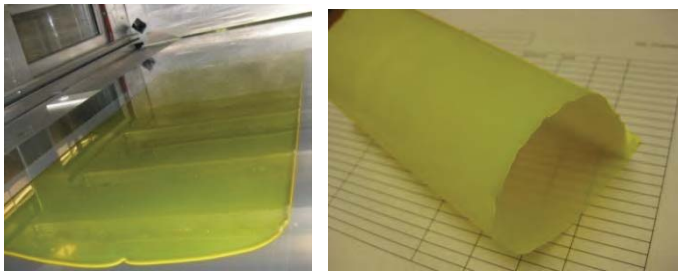

a) b)

Figure 20. a) A polyimide gel film cast with a 12" wide Dr. Blade and a gap of 1.09mm and b) dry polyimide aerogel film.

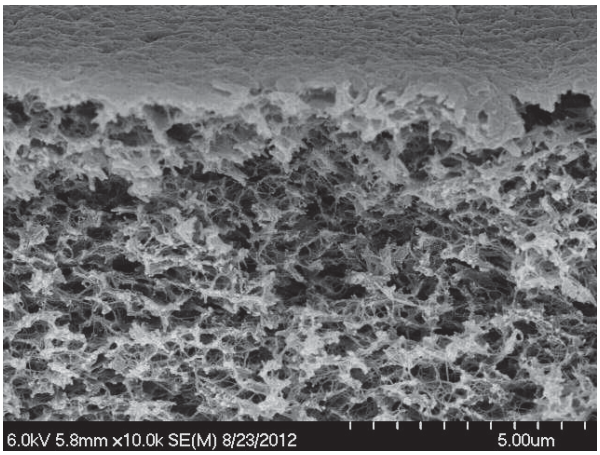

Figure 21. SEM images of cross-section of the aerogel film made with 50 mol% DMBZ and 50 mol% ODA (Reprinted with permission from Publication 6. Copyrights 2012 American Chemical Society).

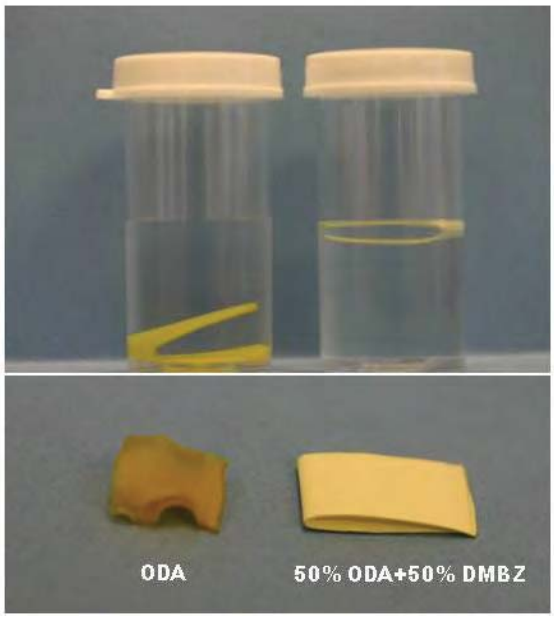

Figure 22. Polyimide aerogel thin films made using 100% ODA (left) and 50 mol% DMBZ + 50 mol% ODA (right) shown in water (top), and after air drying (bottom) (Reprinted with permission from Publication 6. Copyrights 2012 American Chemical Society).

3.2. TAB Cross-linked Polyimide Aerogels (Publication 7)

Instead of using OAPS, 1,3,5-triaminophenoxybenzene (TAB) was used as an alternative approach to cross-link anhydride capped polyamic acid oligomers in NMP. The polyimide aerogels were also fabricated through chemical imidization and supercritical drying. This produces a three dimensional, covalently bonded network structure according to Scheme 8. In this study, the polyimide aerogels have densities range from 0.13 g/cm^3 to 0.34 g/cm^3 and

surface areas as high as 512 m^2/g. Properties of the aerogels from combination of BPDA and PPDA or DMBZ were examined.

Figure 23 shows a pictures of typical TAB cross-linked polyimide aerogels. The TAB cross-linked polyimide aerogels are light yellow to orange yellow in appearance. Thin aerogel films (nominally 0.5 mm) using BPDA and ODA are flexible, whereas thicker parts such as the rectangular prism seen in Figure 23 are rigid and mechanically strong, about 500 times stronger than the conventional silica aerogel. The TAB cross-linked polyimide sol solution is much more viscous, and gels faster than the OAPS cross-linked polyimide sol solution. In order to make the film casting feasible, higher n value or diluting the sol concentration is needed. TAB cross-linked polyimide aerogel film made with ODA, as shown in Figure 23, was cast with a repeat unit n=30 instead of n=25.

Compared to OAPS cross-linked polyimide aerogels, TAB cross-linked polyimide aerogels exhibits slightly higher shrinkages, higher densities, and lower porosities. However, trends due to diamine are the same whether OAPS or TAB is the cross-linker. The highest surface area of the polyimide aerogel is from DMBZ and the lowest from ODA. The most shrinkage exhibited in aerogels made using PPDA and the least shrinkage with DMBZ. Since shrinkage occurs mostly during gelation, this difference is most likely caused by a combination of solvent interactions, chain rigidity, and chain packing. As OAPS cross-linked aerogels, the T_d varies with the diamine used, with the highest T_d seen for the formulations made using PPDA. Formulations made using DMBZ have the lowest T_d due to the loss of the pendant methyl groups. Similar to OAPS cross-linked polyimide aerogels, TAB cross-linked polyimide aerogels made using PPDA as diamine exhibit higher modulus than those made with DMBZ. The film tensile modulus is comparable to that previously reported for the same formulations of OAPS cross-linked aerogels. However, the TAB aerogels, in general, have a higher stress at break than the OAPS cross-linked aerogels. Also the TAB cross-linked polyimide aerogel made with at least 50 mol% DMBZ floats in water and does not shrivel drying in air while the polyimide aerogels using diamine PPDA or more than 50 mol% ODA tend to shrivel in air after soaking in water. All of the polyimide aerogels are possible candidates for high temperature insulation with T_d from 460 to 610°C.

Figure 23. Polyimide aerogels cross-linked with TAB shown fabricated as flexible thin films or molded to a net shape. (Reprinted with permission from Publication 7. Copyrights 2012 American Chemical Society).

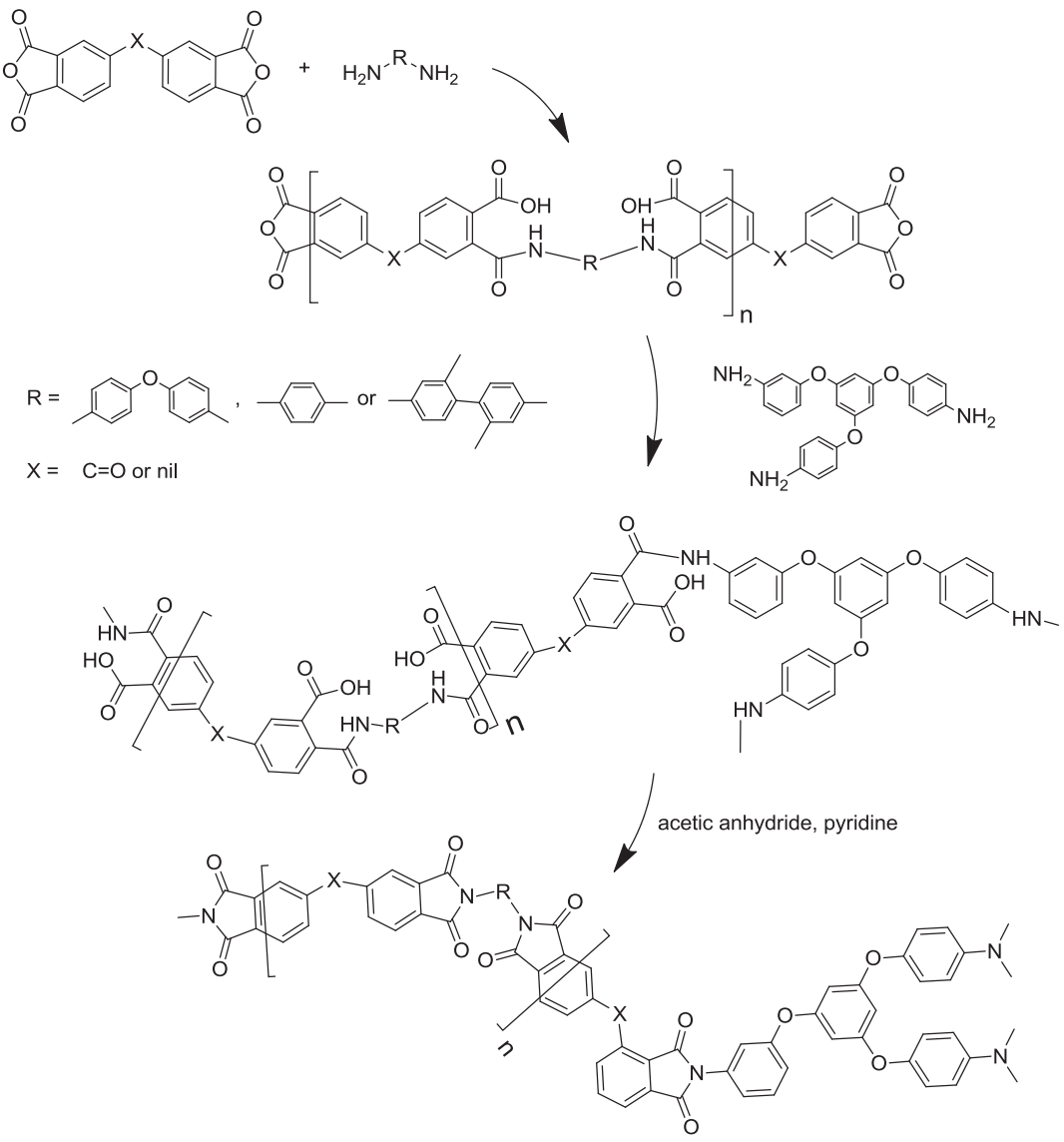

Scheme 8. General synthesis route for polyimide aerogels cross-linked with TAB. (Reprinted with permission from Publication 7. Copyrights 2012 American Chemical Society).

As seen in Figure 24, with a same repeat unit n=25, the TAB cross-linked polyimide aerogels have more densely packed mesostructures than the OAPS cross-linked polyimide aerogels. The TAB cross-linked polyimide aerogel made with DMBZ (Figure 24d) shows larger pore size than other samples with n=25 (Figure 24b, and Figure 24e). For the samples using ODA as diamine, increasing n from 25 (Figure 24b) to 30 (Figure 24c), the porosity around the polyimide fiber strands increases.

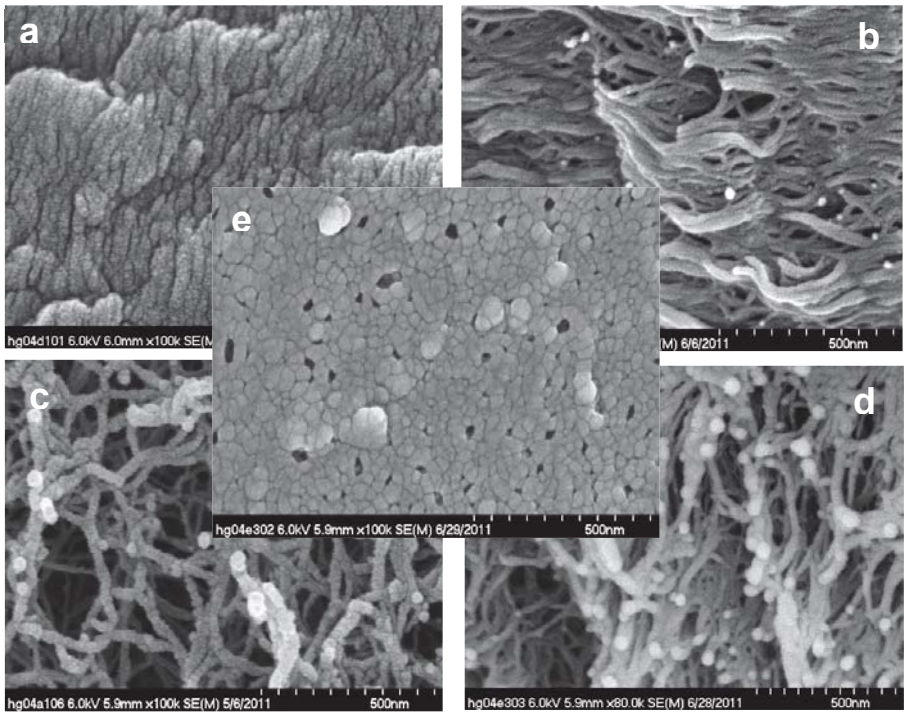

Figure 24. The SEM images of TAB cross-linked polyimide aerogel made with a) PPDA, n=50, b) ODA, n=25, c) ODA, n=30, d) DMBZ, n=25, and e) 50 mol% DMBZ +50 mol% ODA, n=25.

3.3. Applications of Polyimide Aerogels (Publications 3 and 5)

3.3.1 Polyimide Aerogel Films as Inner Thermal Insulation for EDL System (Publication 3)

Small payloads have been handed on Mars by aerodynamic decelerators in the form of hard aeroshells. But for larger aeroshell diameter, an inflatable aerodynamic decelerator, not constrained by the shroud, was suggested. In order to survive the heat of reentry, the inflatable decelerator requests a flexible thermal protection system (TPS) that can endure rigorous handling, high density packing, deployment, and aerodynamic loads. Composite aerogel blankets, Pyrogel 3350 and Pyrogel 2250, developed by Aspen Aerogels, are considered the baseline insulation for the TPS. However, the matrix used in these blankets is fragile and tends to shed silica aerogel particles, which cause trouble to handle and reduce the insulation properties. Polyimide aerogel films have potential usage for the inner thermal insulation for EDL system as a replacement for the composite blankets for they do not shed particles, and have thermal conductivity comparable or lower than the blankets.

Laser Hardened Materials Experimental Lab (LHMEL) and 8' high temperature tunnel (8' HTT) tests were performed on OAPS cross-linked polyimide aerogel film layups. The polyimide aerogels are favorably thermally comparable with Pyrogel 2250 or Pyrogel 3350 silica aerogel blankets. Thermogravimetric analysis (TGA) results show that Pyrogel 3350 begins to outgas at 350°C while the polyimide aerogels have T_d about 560°C to 620°C. As well, the polyimide aerogel films are easier to handle, without breaking down or shedding dust particles.

To simulate heat loads for planetary re-entry, 11 layers of polyimide aerogel films made with BAX (6.75mm) were laid up after two layers of 20mil Nextel 440 BF-20, followed by two 0.5mil Kapton films in LHMEL testing. Thermocouples were placed on surface, on top of first and sixth

layer of insulation and under the last layer. Polyimide aerogel films were able to survive a laser heat flux load of 20 W/cm^2 at 8 torr for 90 seconds, while maintaining a 500 °C difference in temperature measured by thermocouples on the top and under the bottom-most insulation layers. After the test, bottom polyimide aerogel film layer was only darkened, with no hole and no cracks. The advanced insulator layups, utilizing OAPS cross-linked polyimide aerogel films have shown great promise to replace traditional Pyrogel 3350 insulator materials.

3.3.2. Polyimide Aerogels as a Substrate for Lightweight Antennas (Publication 5)

In addition to low density and low thermal conductivity, polyimide aerogels have also been used for their dielectric properties. Among all the cross-linked polyimides with different backbones, a formulation consisting of DMBZ, BPDA, and TAB was selected as a substrate for lightweight antennas due to its low density, low shrinkage, and good mechanical properties, as well as its minimum dielectric constant. This polyimide aerogel has been fabricated for prototype broadband planar patch antennas and benchmarked against state of practice commercial antenna substrates including Rogers Duroid® 6010 and Rogers Duroid® 5880. Results obtained demonstrated that the selected sample has a broader bandwidth, higher gain, and lower mass than the mentioned substrates currently used. Illustrated in Figure 25 are patch antennas with different substrates.

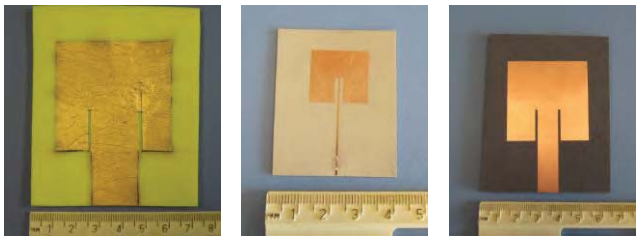

a) b) c)

Figure 25. Photos of patch antennas on a) polyimide aerogel substrate, b) Rogers Duroid® 6010, and c) Rogers Duroid® 5880 (Reprinted with permission from Publication 5. Copyright 2013 American Chemical Society).

4. Synthesis, Characterization, and Processing of Aluminosilicate, Opacified Aluminosilicate Aerogels, and Their Composites (Publications 2, 8, 12)

Although polyimide aerogels and polymer reinforced silica-based aerogels are stronger than the native silica aerogels, their maximum operating temperatures are not suitable for applications above 600^{o}C. Alunimosilicate aerogels densify and sinter at higher temperature than silica aerogels and therefore offer potential application as thermal insulation above 800^{o}C. The objective of this work is to understand how alumina silica ratios, synthesis parameters, and opacifier addition affect aluminosilicate aerogel structures and thermal properties, including densification and sintering.

The aluminum source for preparation of aluminosilicate aerogel can be aluminum alkoxides, aluminum salts, including $AlCl_3$ plus propylene oxide (PO) as a gelling agent, and colloidal dispersions of aluminum hydroxides, such as Boehmite. Our samples of aluminosilicate aerogel were synthesized using Boehmite precursors as the Al source, and TEOS as the Si source. The advantage of using this approach is to avoid using propylene oxide, a very toxic chemical

compound used in the general $AlCl_3$ route, with a hydrolysis rate slower than aluminium organics. The aluminosilicate aerogels produced from Boehmite are different from those produced using $AlCl_3$ and propylene oxide. The Boehmite-derived aluminosilicate aerogels have Al-O-Si groups formed on the Boehmite crystallite surface, from which we can conclude that the backbone of the aerogel is produced by a self-assembly of Boehmite crystallites. They also have fewer tetrahedral AlO4 groups than are obtained by the $AlCl_3$ route. The Boehmite powders used in the study were P2, P2W, L4, T25, and X0, among which P2W has the smallest particle size, as seen in Table 7.

Table 7. Crystallographic characteristics of Boehmite precursors. (With kind permission from Springer Science+Journal of Sol-Gel Science and Technology, "Influence of Ti Addition on Boehmite Derived Aluminum silicate Aerogels: Structure and Properties", 64, **2012**, 367, F. I. Hurwitz, H. Guo, R. B. Rogers, E. J. Sheets, D. R. Miller, K. N. Newlin, M. K. Shave, A. R. Palczer, and M. T. Cox Table 1.)

Boehmite powder	2θ (degree)	d-spacing, (Å)	Crystallite size (nm)
P2w	14.094	6.279	2.6 ± 0.1
P2	14.074	6.287	4.9 ± 0.2
T25	14.168	6.246	6.9 ± 0.1
L4	14.393	6.149	13.0 ± 0.1

T25 gels are very soft and easily broken. Surface area (Figure 26), pore structure, shrinkage and density are strongly influenced by what Boehmite precursor powder is used. Densities of the aluminosilicate aerogels are normally 0.06-0.07g/cm^3. Lowest density, highest surface area and lowest shrinkage are achieved using the smallest particle size P2W powder at an Al:Si ratio of 3:1. The temperature of transformation to mullite shifts to above 1300˚C in the Boehmite-derived system, compared to 980-1005˚C in the $AlCl_3$/PO system. It has been observed that the mesostructures of those aerogels remain stable above 1100^{o}C, as seen in Figure 27.

A radiation opacifier such as TiO_2, when added to SiO_2, can reduce heat transfer at higher temperatures. As reported in literatures, addition of Ti to alumina and mullite systems affects mechanical strength, grain size, and coefficient of thermal expansion. The sol-gel approach was used to incorporate Ti using titanium isopropoxide (TIP) at the molecular level into the aluminosilicate matrix made with Boehmite and TEOS. Tenary Al-Si-Ti aerogels were fabricated successfully using Sasol N.A. P2, P2W, and T25 powders. The ternary system using L4 powder did not gel. Adding Ti has no influence on density, but increases the pore volume which can be attributed to the appearance of larger pores. Ti incorporation also has influence on phase transformation. The Ti containing aluminosilicate aerogels transform to mullite at lower temperature than the corresponding aerogel without Ti, accompanied by loss of pore structure and densification, and formation of larger particle sizes. Using TIP as the Ti source, allowing introduction of Ti into the backbone structure of the gel at the molecular level, but in the ternary aerogel, Ti incorporation is limited to 10 mole percent. This is due to large increases in

viscosity and decreased gelation time with TIP addition. For applications needing higher Ti loadings, the sol-gel approach can also be used to synthesize Al_2TiO_5 aerogels containing 33 percent Ti of the total metal. This formulation was fabricated using P2, P2W, and L4 powders.

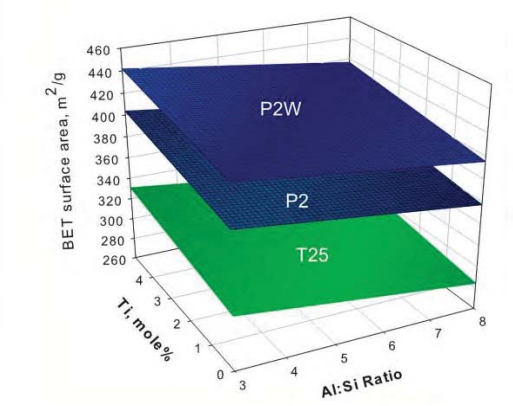

Figure 26. Surface areas of aluminosilicate aerogel using different Boehmite powders. (With kind permission from Springer Science+Journal of Sol-Gel Science and Technology, "Influence of Ti Addition on Boehmite Derived Aluminum silicate Aerogels: Structure and Properties", 64, **2012**, 367, F. I. Hurwitz, H. Guo, R. B. Rogers, E. J. Sheets, D. R. Miller, K. N. Newlin, M. K. Shave, A. R. Palczer, and M. T. Cox Figure 3.)

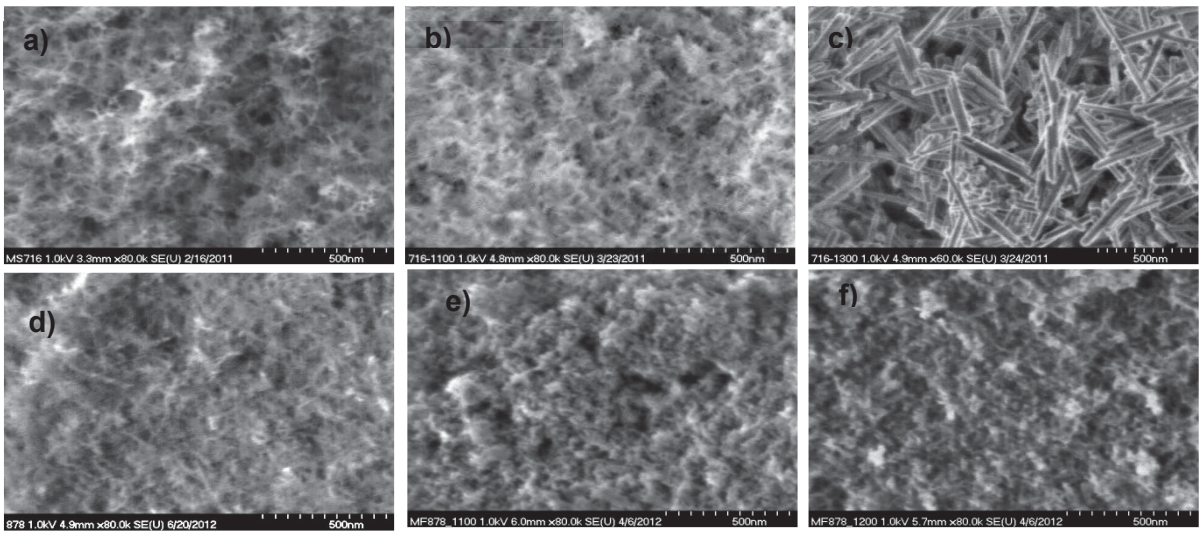

Figure 27. SEM images of (a) The aluminosilicate aerogel (3Al:1Si) made with P2W and after heat treatment at (b) 1100 ^{o}C, and (c) 1300 ^{o}C; and (d) all P2W aerogel, and after heat treatment at (e) 1100 ^{o}C, and (f) 1300 ^{o}C.

Because of the fragile nature of the aluminosilicate aerogel monoliths, we developed a technique to reinforce those using ceramic fabrics, papers, or felts. Alunimosilicate aerogel composites have been prepared using APA-2 alumina paper, Astroquartz silica fiber fabric, and Fiberfrax 972AH alumina paper. Figure 28 shows that a composite made with incorporating aluminosilicate aerogels into APA-2 alumina paper remains flexible. The aluminosilicate aerogel/APA-2 composite has a density of 0.15 g/cm^3, about half of the density of Microtherm

HT (0.3428 g/cm^3). The aluminosilicate aerogel bonds well to the alumina fibers (Figure. 29). The resulted aluminosilicate aerogel composites are much easier to handle than Aspen's composite blankets, Pyrogel 2250 and Pyrogel 3350.

Figure 28. Aerogel composite reinforced with APA-2 paper.

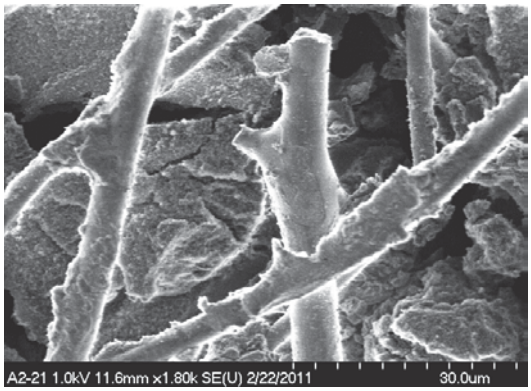

Figure 29. Microstructure of APA-2 with aerogel composite showing good bonding of aerogel to fibers.

5. Overview of the Effort

With the development of the aerospace technology, novel insulation materials with lower thermal conductivity, lighter weight and higher use temperature are required to fit the aerospace application needs. Having nanosize pores and high porosity, aerogels are superior thermal insulators among other things. Our research goal was to develop aerogels with mechanical and environmental stability that suitable for a variety of aeronautic and space applications. In the past six years, several different types of aerogels, including polymer hybrid silica-based, polyimide and inorganic aerogels have been formulated, fabricated, and characterized. Much success has led to the scale-up process for testing for different applications such as insulations for cryotanks for advanced space propulsion systems, inflatable aerodynamic decelerators for EDL operations, and antennas in aircrafts and other airborne platforms.

The overall achievements of this effort to date include

- The milestones achieved and delivered have far exceeded expectations
- Several papers, talks and posters have been published and presented
- Two patents were granted
- Five disclosures have been filed
- Three awards, Exceptional Space Act Award, R&D and Nortech Innovation, were received
- Several recognitions have been acknowledged
- A total of 1,557 aerogel samples have been examined and 23,202 SEM images were taken and edited.
- Large components have been produced beyond the lab-scale
- Tests for actual applications have been conducted on a small scale
- Generating interests from 51 companies, institutions and government centers
- Mentoring and training several interns from different programs including LERCIP, USRP, MUST and INSPIRE.

6. Future Work

Further investigation and advanced studies of these on-going developments are essential. The proposed tasks and their delivery dates are described below.

1. Polymer Hybrid (cross-linked) Silica-based and Fiber-spun Silica Aerogels

Our extensive studies have been focused on improving physical and mechanical properties of non-reinforced, or native, silica aerogels by cross-linking the skeletal structures of silica gels with organic polymers, as well as embedding nano-materials into the silica gels. Results thus far have shown an improvement in physical and mechanical properties of these systems.

1.1. Completed the study of aerogel system cross-linked with polystyrene at different molecular weights (6//30/2008)

1.2. Completed the studies on developing

1.2.1. Flexible, polymer cross-linked (hybrid) silica-based aerogels with different silica-based precursors and with different polymers (6/30/2009)

1.2.2. Flexible nano fiber reinforced silica aerogels (6/30/2009)

1.2.3. Completed the study of polyimide and clay-reinforced polyimide cross-linked silica-based aerogels (6/30/2012)

1.3. Completed the study of one-pot cross-linked aerogels (6/30/2009)

2. Cross-linked polyimide aerogels

While polymer cross-linked silica-based aerogels are potentially suitable for low temperature applications, higher temperature stability is required for a variety of aeronautic and space applications such as space suit insulation for planetary surface missions, insulation for inflatable structures for habitats, inflatable aerodynamic decelerators for EDL operations. One of the

organic aerogel types that has been investigated at Glenn involves the development of polyimide aerogels, both monoliths and flexible thin films, due to their thermal stability up to 450°C when compared to most organic polymers.

2.1. Completed identifying and optimizing aerogel systems that show potential use for commercialization (6/30/2011)

2.1.1. Completed fabricating and building cross-linked polyimide aerogel as an insulating material for cryotanks. Products were delivered to NASA Marshall Space Flight Center (4/30/2012)

2.1.2. Completed fabricating different sizes of TAB cross-linked polyimide for Antenna project (Phase 1) (6/30/2012)

2.1.3. Completed the scale-up process to produce polyimide aerogel films at the University of Akron (6/30/2013). Seeking Industry scale up is on-going.

2.1.4. In progress of scaling-up the process for Antenna project (Phase 2) (On-going, 85 % completed)

2.2. Examining and testing the polyimide aerogel films for inflatable aerodynamic decelerators

2.2.1. Completed the LHMEL and Langley 8' wind tunneling tests (6/30/2013)

2.2.2. In progress of using Boeing LCAT test (On-going)

3. Aluminosilicate and opacified aluminosilicate aerogels

Although polymer hybrid silica-based and polyimide aerogels have found been to be much stronger than the native, or non-cross-linked, silica aerogel, they are inapplicable for uses at higher temperatures above 600°C. Other types of inorganic aerogels have been investigated such as Aluminosilicate aerogels which densify and sinter at temperature above 800°C.

3.1. Completed fabricating Aluminosilicate aerogel using Boehmite powder as Aluminum precursor (6/30/2012)

3.2. Completed studying the effect of using opacifiers in the aluminosilicate aerogels and their overall properties (6/30/2012).

3.3. Completed fabricating and improving the aluminosilicate aerogel/APA-2 composites with better thermal stability ability (6/30/2013). Several other kinds of ceramic papers, felts, and ceramic oxide foams were used to make aluminosilicate aerogel composites. (On-going)

7. Patents

1. H. Guo and M. A. B. Meador “Polyalkylene imide aerogel”, **LEW-19108-1**, 2013.
2. B. N. Nguyen and M. A. B. Meador *U.S. Patent No. 8,314,201*, “Highly porous ceramic oxide aerogels having improved flexibility,” November 20, 2012.
3. B. N. Nguyen, H. Guo, and M. A. B. Meador *U.S. Patent No. 8,258,251*, U.S. Continuation-in-Part Application for “Highly porous ceramic oxide aerogels having improved flexibility,” September 4, 2012.
4. F. Hurwitz, D. R. Miller, H. Guo, and M .G. Fields “Method for Fabricating Aerogel Paper, Felt or Fabric Reinforced Composites” **LEW-18971-1, 2012.**
5. M. A. B. Meador and H. Guo, “Porous Cross-linked Polyimide Networks” **OAI 48786US1, LEW-18864-1, US patent application** No. 61/594,657, February 3, 2012.
6. G. Sauti, T.-B. Xu, E. J. Siochi, S. Wilkinson, M. A. Meador, and H. Guo “Robust, Flexible and Lightweight Dielectric Barrier Discharge Actuators using Nanofoams/Aerogels**” LAr 18189-1, 2012.**
7. B. N. Nguyen and M. A. B. Meador “High temperature, flexible and foldable polyimide aerogels with high mechanical properties,” **LEW-18825-1**, 2010.

7. Awards

1. Exceptional Space Act Award (M. A. B. Meador and H. Guo)
2. 2013 Nortech Innovation Award (M. A. B. Meador and H. Guo)
3. 2012 100 R&D Award from R&D megazine (M. A. B. Meador and H. Guo)

8. Recognitions

1. Chemical Engineering news “Polymer Aerogels Provide Insulation For Earth and Space”, 2012, 90, 30-31.
2. R&D magazine, “A Tougher Aerogel”, Aug. 12, 2012
3. Tech Brief LEW-18864-1
4. Tech Brief LEW-17685
5. Plain Dealer “Ohio Aerospace Institute explores earthly uses for space-age ideas”, March 6, 2007.
6. B. N. Nguyen, M. A. B. Meador, S. L. Vivod, and M. E. Tousley *NASA Glenn Research Center R&T* “Flexible Crosslinked Aerogels,” 2007.
7. M. A. B. Meador, B. N. Nguyen, and G. Gould *NASA Glenn Research Center R&T* “Manufacturing Process for Polymer Crosslinked Aerogel Composites Developed,” 2007.

9. Conference Presentations

1. M. A. B. Meador, H. Guo, and N. J. Mesick "Polyimide Aerogels for Use as Insulation for Inflexible Thermal Protection System for Inflatable Aerodynamic Decelerators", 246th ACS meeting, 2013, Indianapolis, IL.
2. M. A. B Meador, F. A. Miranda, S. Wright, A. Snadberg, B. N. Nguyen, F. W. VanKeuls, C. H. Mueller, and R. Rodriguez-Sokis "Low Dielectric Polyimide Aerogels as a Substrate for Patch Lightweight Antennas" Porous Polymers Symposium, American Chemical Society Spring National Meeting, New Orleans, Louisiana, April 7-11, 2013.
3. F. I. Hurwitz, R. B. Rogers, and H. Guo "High Temperature Aluminosilicate Aerogel Based Composites for TPS", Gordon Conference, 2013.
4. F. I. Hurwitz and H. Guo "Thermal Performance of Flexible, High Temperature Aerogel Composite Insulation", NSMMS meeting, June 24-27, 2013, Bellevue, WA.
5. H. Guo, M. A. B. Meador, S. Bali, L. McCokle, J. Guo, B. Hamilton, and M. Cakmak "Optimization of properties of cross-linked polyimide aerogels for high temperature aerospace applications", 245th ACS meeting, 2013, New Orleans, LA.
6. M. A. B Meador, F. A. Miranda , S. Wright, A. Snadberg, B. N. Nguyen, F. W. VanKeuls, C. H. Mueller, and R. Rodriguez-Sokis "Low Dielectric Polyimide Aerogels as a Substrate for Patch Lightweight Antennas", *Porous Polymers Symposium, American Chemical Society Spring National Meeting,* 245th ACS meeting, 2013, New Orleans, LA.
7. H. Guo, M. A. B. Meador, D. A. Scheiman, and L. McCorkle "Octa(aminophenyl) Silsesquioxane (OAPS) Cross-Linked Polyimide Aerogels", Fall MRS meeting, Nov., 2012, Boston, MA.
8. M. A. B. Meador, S. L. Vivod, H. Guo, and B. N. Nguyen "Development of Flexible, Polyimide Aerogel Insulation for Hypersonic Inflatable Aerodynamic Decelerators", 9th International planetary Probe Workshop, Toulouse, France, June 18-22, 2012.
9. J. A. Del corso, W. E. Bruce, III, S. J. Hughes, J. A. Dec, M. D. Rezin, M. A. B. Meador, H. Guo, D. G. Fletcher, A. M. Calomino, and F. M. Cheatwood "Flexible Thermal Protection System Development for Hypersonic Inflatable Aerodynamic Decelerators", 9th International Planetary Probe Workshop, June 16-22, 2012, Toulouse, France
10. F. I. Hurwitz, M. Shave, M. Fields, A. Palczer, D. Johnson, R. Rogers, and H. Guo "Development of Aerogel Composites for Multilayer Insulation, Thermoelectric Applications and High Temperature Thermal Protection Systems", NMMS meeting, 2012.
11. F. I. Hurwitz, M. K. Shave, D. R. Miller, K. N. Newlin, M. T. Cox, R. B. Rogers, A. R. Palczer, and H. Guo "GRAAFiTI (Glenn Research Center Aluminosilicate Aerogel Fiber-reinforced Thermal Insulation) Felts for Space Exploration", NSMMS meeting, June, 2011, Madison, WI.
12. H. Guo, M. A. B. Meador, L. McCorkle, D. J. Quade, A. Palczer, D. A. Scheiman, J. Guo, B. H. Hamilton, M. Cakmak, and G. Sprowl "Polyimide Aerogels with Amine Functionalized Polysilsesquioxane Cross-links", 241th ACS meeting, Mar., 2011, Anaheim, CA.
13. B. N. Nguyen, M. A. B. Meador, S. Ercegorvic, M. Rohovie, L. McCorkle, J. Guo, L. Li, B.H. Hamilton, and D.J. Quade "Development of high temperature, flexible polyimide aerogels", 241th ACS meeting, Mar., 2011, Anaheim, CA.

14. F. I. Hurwitz, H. Guo, and K. N. Newlin "Influence of Bohmite Precursor on Aluminosilicate Aerogel Pore Structure, Phase Stability and Resistance to Densification at High Temperatures", 241st ACS National Meeting & Exposition, March 27-31, 2011, Anaheim, CA.

15. M. A. B Meador, S. L. Vivod, H. Guo, and B. N. Nguyen "Tailoring Properties of Aerogels for Aerospace Applications", (proceeding and presentation), 241th ACS meeting, Mar., 2011, Anaheim, CA.

16. J. Guo, B. N. Nguyen, L. Li, M. A. B. Meador, and M. Cakmak "Clay Reinforced Polyimide/Silica Hybrid Aerogel", 241th ACS meeting, Mar., 2011, Anaheim, CA.

17. F. I. Hurwitz, H. Guo, E. J. Sheets, D. R. Miller, and K. N. Newlin "Tailoring of Boehmite-Derived Aluminosilicate Aerogel Structure and Properties: Influence of Ti Addition", Fall MRS meeting, Nov. 28-Dec. 1, 2010, Boston, MA.

18. M. A. B. Meador, B. N. Nguyen, and H. Guo "Polyimide Aerogels with 3-D Cross-linked Structure", Fall MRS meeting, Nov. 28-Dec. 1, 2010, Boston, MA.

19. H. Guo, B. N. Nguyen, B. Shonkwiler, and M. A. B. Meador "Hydrophobic, low density aerogels with improved elastic properties", 239th ACS meeting, Mar. 2010, San Francisco, CA.

20. M. A. B. Meador, E. Malow, Z. J. He. L. McCorkle, H. Guo, and B. N. Nguyen "Synthesis and Properties of Nanoporous Polyimide Aerogels having a Covalently Bonded Network Structure", 239th ACS meeting, Mar. 2010, San Francisco, CA.

21. S. L. Vivod, M. A. B. Meador, and B. N. Nguyen "Bismaleimide Reinforced Silica Aerogels via Surface Modification through Incorporation of p-Aminophenyltrimethoxysilane", 239th ACS meeting, Mar. 2010, San Francisco, CA.

22. M. A. B. Meador, E. J. Malow, Z. He, L. McCorkle, and B. N. Nguyen "Synthesis and Properties of Nanoporous Three-Dimentinal Cross-linked Polyimide Aerogels", 239th ACS meeting, Mar. 2010, San Francisco, CA.

23. M. A. B. Meador, E. Malow, Z. He, B. N. Nguyen, H. Guo, and L. S. McCorkle "Polyimide Aerogels for High Temperature Insulation Applications", *High Temperature Polymeric Laminate (High Temple) Workshop,* January 31 – February 5, 2010, Destin, Florida.

24. B.N. Nguyen, M. A. B. Meador, A. Medoro, B. Shonkwiler, and L. McCorkle "Tailoring elastic properties of silica aerogels cross-linked with an isocyanate", 237th ACS meeting, Mar. 2009, Salt Lake city, UT.

25. H. Guo, B. N. Nguyen, D. A. Scheiman, and M. A. Meador "Flexible Aerogels Synthesized by Bis[3-(Triethoxysilyl)propyl]disulfide and Diglycidyl Ether Terminated Poly(dimthylsiloxane)", 237th ACS meeting, Mar. 2009, Salt Lake city, UT.

26. H. Guo, D. A. Scheiman, B. N. Nguyen, and M. A. Meador "Bis[3-(Triethoxysilyl)propyldisulfide] Derived Silica Aerogel", 235th ACS meeting, Apr. 2008, New Orleans, LA.

27. S. Vivod, M. A. B. Meador, B. N. Nguyen, D. Quade, and J. Randall "Di-isocyanate crosslinked aerogels with 1,6-bis(trimethoxysilyl)hexane incorporated in silica backbone", 235th ACS meeting, Apr. 2008, New Orleans, LA.

28. B. N. Nguyen, M. A. B. Meador, M. E. Tousley, and B. Shonkwiler "Improving Flexibility of Silica-Based Aerogels Crosslinked with Polystyrene", 235th ACS meeting, Apr. 2008, New Orleans, LA.

29. M. A. B. Meador, B. N. Nguyen, and S. L. Vivod "Recent Advances in Cross-linking Silica Aerogels with Polymers," 235th ACS meeting, Apr. 2008, New Orleans, LA.

10. Publications

1. J. Guo, B. N. Nguyen, L. Li, M. A. B. Meador, D. A. Scheiman, and M. Cakmak "Clay reinforced polyimide/silica hybrid aerogel" *J. Mater. Chem. A*., **2013**, 1, 7211.
2. F. I. Hurwitz, H. Guo, R. B. Rogers, E. J. Sheets, D. R. Miller, K. N. Newlin, M. K. Shave, A. R. Palczer, and M. T. Cox "Influence of Ti Addition on Boehmite Derived Aluminum silicate Aerogels: Structure and Properties" *J. Sol-gel Sci*., **2012**, 64:367
3. J. A. Del corso, W. E. Bruce, III, S. J. Hughes, J. A. Dec, M. D. Rezin, M. A. B. Meador, H. Guo, D. G. Fletcher, A. M. Calomino, and F. M. Cheatwood "Flexible Thermal Protection System Development for Hypersonic Inflatable Aerodynamic Decelerators" 9th International Planetary Probe Workshop, 16-22 JUNE **2012**, TOULOUSE
4. M. A. B. Meador, S. L. Vivod, H. Guo, and B. N. Nguyen "Development of Flexible, Polyimide Aerogel Insulation for Hypersonic Inflatable Aerodynamic Decelerators" 9th International planetary Probe Workshop, Toulouse, France, June 18-22, **2012**.
5. M. A. B Meador, F. A. Miranda, S. Wright, A. Snadberg, B. N. Nguyen, F. W. VanKeuls, C. H. Mueller, and R. Rodriguez-Sokis "Low Dielectric Polyimide Aerogels as a Substrate for Patch Lightwieght Antennas" *Appl. Mater. & Inter.*, **2012**, 4, 6346.
6. H. Guo, M. A. B. Meador, L. McCorkle, D. J. Quade, J. Guo, B. Hamilton, and M. Cakmak "Tailoring Properties of Cross-linked Polyimide Aerogels for better Moisture Resistance, Flexibility and Strength" *ACS Appl. Mater. Inter.,* **2012,** 4, 5422.
7. M. A. B. Meador, E. J. Malow, R. Silva, S. Wright, D. Quade, S. L. Vivod, H. Guo, J. Guo, and M. Cakmak "Mechanically Strong, Flexible Polyimide Aerogels Cross-Linked with Aromatic Triamine" *ACS Appl. Mater. Interfaces*, **2012**, 4, 536.
8. F. I. Hurwitz, H. Guo, E. J. Sheets, D. R. Miller, and K. N. Newlin "Tailoring of Boehmite-Derived Aluminosilicate Aerogel Structure and Properties: Influence of Ti Addition**"** *Mater. Res. Soc. Symp. Proc.* Vol. 1306 © **2011** Materials Research Society, DOI: 10.1557/opl.2011.95.
9. H. Guo, M. A. B. Meador, L. McCorkle, D. J. Quade, J. Guo, B. Hamilton, M. Cakmak, and G. Sprowl "Polyimide Aerogels Cross-Linked through Amine Functionalized Polyoligomeric Silsesquioxane" *ACS App. Mater. Inter.*, **2011**, 3, 546.
10. H. Guo, M. A. Meador, and G. Sprowl "Polyimide Aerogels with Amine Functionalized Polysilsequioxane Crosslinks" *Polymer Prep.,* **2011**, 52, 253.
11. B. N. Nguyen, M. A. B. Meador, S. Ercegorvic, M. Rohovie, L. McCorkle, J. Guo, L. Li, B. H. Hamilton, and D. J. Quade "Development of high temperature, flexible polyimide aerogels" *Polymer Prep.*, **2011**, *52*, 256.
12. F. I. Hurwitz, H. Guo, and K. N. Newlin "Influence of Bohmite Precursor on Aluminosilicate Aerogel Pore Structure, Phase Stability and Resistance to Densification at High Temperatures" *Polymer Prep.*, **2011**, 52, 16.
13. S. L. Vivod, M. A. B. Meador, M. Cakmak, and H. Guo "Carbon Nanofiber/polyimide Aerogel Thin Film Composites" *Polymer Prep.,* **2011**, 52, 127.
14. J. Guo, B. N. Nguyen, L. Li, M. A. B. Meador, and M. Cakmak "Clay Reinforced Polyimide/Silica Hybrid Aerogel" *Polymer Prep.*, **2011**, 52, 259.
15. M. A. B Meador, S. L. Vivod, H. Guo, and B.N. Nguyen "Tailoring Properties of Aerogels for Aerospace Applications" *Polymer Prep*., **2011**, 52, 134. (proceeding and presentation)

16. M. A. B. Meador, E. Malow, Z. J. He, L. McCorkle, H. Guo, and B. N. Nguyen "Synthesis and Properties of Nanoporous Polyimide Aerogels having a Covalently Bonded Network Structure" *Polymer Prep*., **2010**, 51, 265.

17. H. Guo, B. N. Nguyen, L. S. McCorkle, B. Shonkwiler, and M. A. B. Meador "Hydrophobic, low density aerogels with improved elastic properties" *Polymer Prep*, **2010**, 51, 602.
18. M. A. B Meador, C. M. Scherzer, S. L. Vivod, D. Quade, and B. N. Nguyen "Epoxy Reinforced Aerogels Made Using a Streamlined Process" *Appl. Mater. & Inter.*, **2010**, 2, 2162.

19. B. N. Nguyen, M. A. B. Meador, A. Medoro, V. Arendt, J. Randall, L. McCorkle, and B. Shonkwiler "Elastic Behavior of Methyltrimethoxysilane Based Aerogels Reinforced with Tri-isocyanate" *Appl. Mater. & Inter.*, **2010**, 2, 1430.

20. S. L. Vivod, M. A. B. Meador, and B. N. Nguyen "Bismaleimide Reinforced Silica Aerogels via Surface Modification through Incorporation of p-Aminophenyltrimethoxysilane" *Polymer. Prep.*, **2010**, 51, 646.

21. H. Guo, B.N. Nguyen, L.S. McCorkle, B. Shonkwiler, and M.A.B. Meador "Hydrophobic, Low Density Aerogels with Improved Elastic Properties" *Polymer Prep.*, **2010**, 51, 602.

22. M. A. B. Meador, E. Malow, Z. He, B. N. Nguyen, H. Guo, and L. S. McCorkle "Polyimide Aerogels for High Temperature Insulation Applications" *High Temperature Polymeric Laminate (High Temple) Workshop,* Destin, Florida, January 31 – February 5, **2010**.

23. L. Li, B. Yalcin, B. N. Nguyen, M. A. B. Meador, and M. Cakmak "Flexible Nanofiber Reinforced Aerogel(Xerogel) Synthesis, Manufacture and Characterization" *Appl. Mater. & Inter.*, **2009**, 1, 2491.

24. H. Guo, B. N. Nguyen, L.S. McCorkle, B. Shonkwiler, and M. A. B. Meador "Elastic Low Density Aerogels Derived from Bis[3-(Trimethoxyl)Propyl]Disulfide, Tetramethylorthosilicate and Vinyltrimethoxysilane Via a Two-step Process" *J. of Mater. Chem.*, **2009**, 19. 1.

25. M. B. A. Meador, A. S. Weber, A. Hindi, M. Naumenko, L. McCorkle, D. Quad, S. L. Vivod, G.L. Gould, S. White, and K. Deshpande "Structure-Property Relationship in Porous 3D Nanostructures: Epoxy-Cross-linked Silica Aerogels Produced Using Ethanol as the Solvent" ACS *Appl. Mater. & Inter.*, **2009**, 1, 894.

26. B. N. Nguyen, M. A. B. Meador, M. E. Tousley, B. Shonkwiler, L. McCorkle, D.A. Scheiman, and A. Palczer "Tailoring Elastic Properties of Silica Aerogels Cross-Linked with Polystyrene" ACS *Appl. Mater. & Inter.*, 2009, 1, 621.

27. B. N. Nguyen, M. A. B. Meador, A. Medoro, B. Shonkwiler, and L. McCorkle "Tailoring elastic properties of silica aerogels cross-linked with an isocyanate" *Polymer Prep.*, **2009**, 50, 370.

28. S. Vivod, M. A. B. Meador, B. N. Nguyen, and R. Perry "Di-isocyanate cross-linked silica aerogels with hexyl link incorporated into the underlying silica backbone" *Polymer Prep.*, **2008**, 50, 119.

29. S. Vivod, M. A. B. Meador, B. N. Nguyen, D. Quade, and J. Randall "Di-isocyanate crosslinked aerogels with 1,6-bis(trimethoxysilyl)hexane incorporated in silica backbone" *Polymer. Prep.*, **2008**, 491, 521.

30. B. N. Nguyen, M. A. B. Meador, M. E. Tousley, and B. Shonkwiler "Improving Flexibility of Silica-Based Aerogels Crosslinked with Polystyrene" *Polymer Prep.*, **2008**, 41, 225.

31. M. A. B. Meador, B. N. Nguyen, and S.L. Vivod "Recent Advances in Cross-linking Silica Aerogels with Polymers" *Polymer Prep.*, **2008**, 41, 225.

11. List of Tables

12. List of Schemes

13. List of Figures

References

1. (a) Jones, S. M., *J. Sol–Gel Sci. Technol*. **2006**, *40*, 351,-357. (b) Fesmire, F. E., *Cryogenics*, **2006**, *46*, 111-117. (c) Pierre, A. C.; Pajonk, G. M., *Chem. Rev*. **2002**, *102*, 4243-4265.
2. Moner-Girona, M.; Roig, A;Molins, E.; Martínez,E.; Esteve, J. *J. Appl. Phys. Lett.* **1999**, *75*, 653-655.
3. Tang, H. H.; Orndoff, E. S.; Tevino, L. A. Presented at the *International Conference On Environmental Systems Technical Papers,* Paper No. 2006-01-2235.
4. Braun, R. D.; Manning, R. M. *J. Spacecr. Rockets* **2007**, *44*, 310-323.
5. Smith, B. P.; Tanner, C. L.; Mahzari, M.; Clark, I. G.; Braun, R. D.; Cheatwood, F. M. Presented at the *2010 IEEE Aerospace Conference,* Big Sky, MT; IEEE: Piscataway, NJ, 2010; Paper No. IEEEAC 1273.
6. Smith, B. P.; Clark, I. G.; Braun, R. D. Presented at the *2011 IEEE Aerospace Conference*, Big Sky, MT; IEEE: Piscataway, NJ, 2011; Paper No. IEEEAC 1312.
7. a) Ilhan, U. F.; Fabrizzio, E. F., McCorkle, L.; Scheiman, D. A.; Dass, A.; Palczer, A.; Meador, M. A. B.; Johnston, J. C.; Leventis, N. *Mater. Chem.* **2006**, *16*, 3046-3054. (b) Mulik, S.; Sotiriou-Leventis, C.; Churu, G.; Lu, H.; Leventis, N. *Chem. Mater*. **2008**, *20* (*15*), 5035–5046.
8. Meador, M. A. B.; Fabrizzio, E. F.; Ilhan, F.; Dass, A.; Zhang, G.; Vassilaras, P.; Johnston, J. C.; Leventis, N. *Chem. Mater.* **2005**, *17*, 1085.
9. Boday, D. J.; Stover, R. J.; Muriithi, B.; Keller, M. W.; Wertz, J. T.; Obrey, K. A. D.; Loy, D. A. *ACS Appl. Mater. Interfaces*, **2009**, *1* (7), pp 1364–1369.
10. Brown, G. J.; Lingard, JJ. S.; Darley, G.D.; Underwood, J. C. 19*th AIAA Aerodynamic Decelerator System Tecnology Conference and Seminar;* Williamsburg, VA, May 21-24, 2007; AIAA: Reston, VA, 2007; 2543.
11. Hench, L.; West, J. *Chem. Rev.* **1990**, 33-72.
12. Emmerling, A.; Gross, J.; Gerlach, R.; Goswin, R.; Reichenau-er, G.; Fricke, J.; Haubold, H.-G. *J. Non-Cryst. Solids* **1992**, 125, 230-243.
13. Saliger, R.; Heinrich, T.; Gleisser, T.; Fricke, J. *J. Non-Cryst. Solids* **1995**, 186, 113-117.